AN ELECTRICAL MODEL FOR A TRANSDUCER USED IN THE STUDY OF ACOUSTIC EMISSION FROM MATERIALS UNDER TENSILE STRESS

Huynh Huu Le

A Thesis

Submitted To The Faculty Of Graduate Studies

In Partial Fulfillment Of The Requirements For The Degree

Of Master Of Science

Electrical Engineering Department

University of Manitoba

Winnipeg, Manitoba

May 1972

AN ELECTRICAL MODEL FOR A TRANSDUCER USED IN THE STUDY OF ACOUSTIC EMISSION FROM MATERIALS UNDER TENSILE STRESS

by

Huynh Huu Le

ABSTRACT

A method for modeling a transducer used in the study of acoustic emission from materials under tensile stress is described in this thesis. The method involves the measurement of the input impedance of the transducer over a wide range of frequencies from which one derives the electrical elements of the model. The model is then used in the electrical analysis of the system. As an illustrative example, the present technique is applied to determine the electrical model of an actual transducer (Dunegan Research Corporation, single-ended model) used in the study of acoustic emission from Fe 3% Si specimens. This model together with the model for the preamplifier used in the actual system makes possible the computation of the impulse response which relates the output waveform and the output statistical properties to the input waveform and the input statistical properties.

ACKNOWLEDGEMENT

The author wishes to express deep gratitude to his thesis advisor Dr. G.O. Martens, for suggesting the thesis topic as well as for his guidance and supervision throughout the project.

LIST OF FIGURES

LIST OF GRAPHS

LIST OF PHOTOGRAPHS

TABLE OF CONTENT

CHAPTER I

INTRODUCTION

The study of acoustic emission from materials under tensile stress requires the use of the system shown in Fig. 1. Such a system consists of a piezoelectric transducer, a preamplifier, a wide-band amplifier and a tape recorder to store the signal.

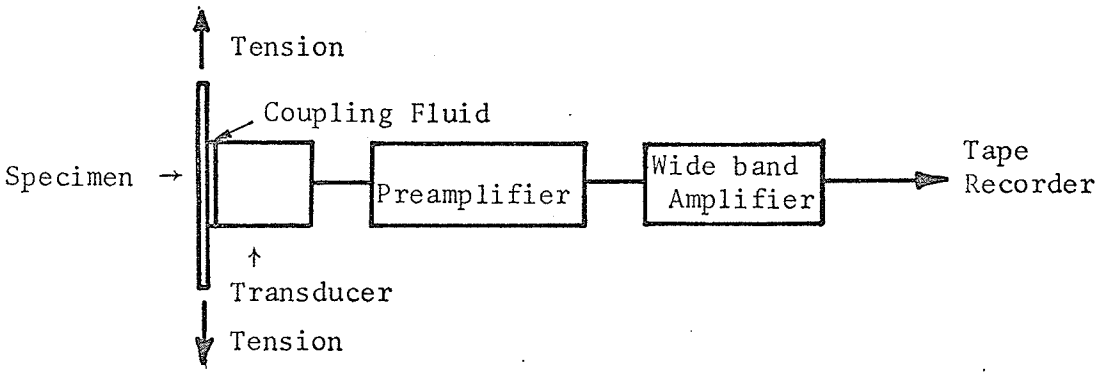

Fig. 1. System used in the study of acoustic emission from materials under tensile stress.

In order to be able to analyze the system by electrical network theory, the modeling of the piezoelectric transducer by lumped passive electrical components is required. Such attempts have been proposed by researchers in the field of dynamical analogies, namely Mason [1] - [2], Beranek [3], Kinsler and Frey [4]. To summarize, a piezoelectric transducer is just an electromechanical transducer for converting electrical energy into mechanical energy, and vice versa. Piezoelectricity has been discussed

by Cady [5]. An electromechanical transducer can be represented [4] by a four-terminal network with two electrical input terminals (voltage E and current I) and two mechanical output terminals (force F and velocity V) as shown in Fig. 2.

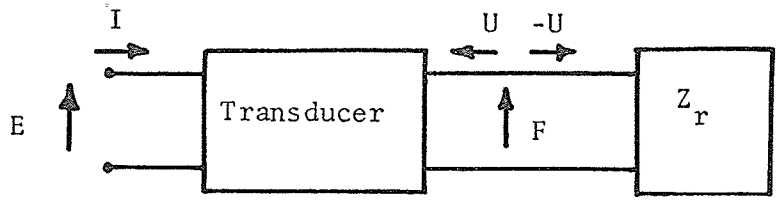

Fig. 2. Four terminal electromechanical network of transducer with attached acoustic load Z_r.

According to Kinsler and Frey [4], the equivalent circuit of the piezoelectric transducer is as shown in Fig. 3 where R_o is the dielectric leakage resistance, L the electrical equivalent of the effective mass in vibration, C the electrical equivalent of the effective mechanical compliance, R the electrical equivalent of the mechanical friction and C_o the electrostatic capacitance between the two electrical input terminals when the crystal is not vibrating.

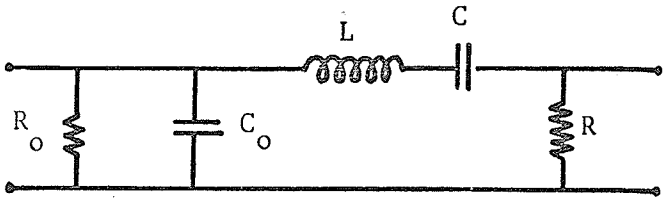

Fig. 3. Equivalent circuit of piezoelectric transducer.

The magnitudes of R_o, C_o, L, C and R depend upon the way in which the transducer is built. For some cases, these calculations are easily made from the properties of the transducer [1]. Methods of measuring these equivalent electrical parameters involving only the measurement of the impedance have been described by various papers [6] - [8].

Thus it is possible to replace the transducer by a linear time-invariant electrical equivalent circuit. The present thesis offers a method of modeling which involves the measurement of the impedance over a wide range of frequencies. From the model, possible applications are derived by considering the overall transfer function of the original system which can be found by additional modeling of the preamplifier. In other words, we are able to analyze the system by using the tools of linear system analysis. From the experimental curve, we will choose some particular points which determine the possible values of the principal parameters of the equivalent circuit. Different theoretical curves derived from these possible sets of values will be compared, either analytically or visually, with the experimental curve. We next describe certain criteria which help to select an acceptable curve and hence the acceptable values for the parameters.

The second chapter deals with the method of modeling the transducer and an actual transducer (Dunegan Research Corporation, single-ended model) is given as an example of application of the method.

The third chapter will deal with the computation of the impulse response of the system which one may derive when the model has been determined. This is the main purposes for obtaining a model of the transducer. Once the impulse response of the entire system has been found, the unknown input waveform and its statistical properties may be obtained from the observed output waveform and its statistical properties.

CHAPTER II

METHOD OF MODELING

A. *Input Impedance of the Electrical Model.*

In general, the dielectric leakage resistance R_o is so large (in the order of 10^{12} ohms) that we may neglect it. The expression for the input impedance of the remaining circuit shown in Fig. 4 is given by [6]:

$$Z(j\omega) = \frac{1}{j}\ \frac{\omega_s}{\omega}\ \frac{RQ}{r}\ \frac{1 + j\,Q\left(\frac{\omega}{\omega_s} - \frac{\omega_s}{\omega}\right)}{1 + j\,Q\sqrt{\frac{1+r}{r}}\left(\frac{\omega}{\omega_p} - \frac{\omega_p}{\omega}\right)} \qquad (1)$$

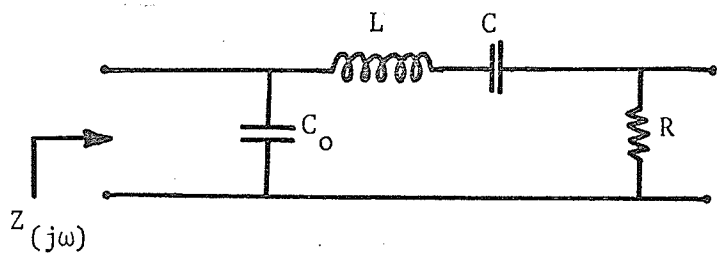

Fig. 4. Simplified electrical model of the transducer.

where:

$$r = \frac{C_o}{C}$$

$$\omega = 2\pi f\ ,\quad \omega_s = 2\pi f_s\ ,\quad \omega_p = 2\pi f_p$$

$$f_s = \frac{1}{2\pi\sqrt{LC}} \quad \text{(series resonance frequency)}$$

$$f_p = \frac{1}{2\pi}\sqrt{\frac{1}{LC}\left(1 + \frac{1}{r}\right)} \quad \text{(parallel resonance frequency)}$$

$$Q = \frac{\omega_s L}{R} \quad \text{(quality factor)}$$

We note that $Z(j\omega)$ is a complex quantity which can be written as:

$$Z(j\omega) = |Z(\omega)| \angle \theta(\omega) = R(\omega) + j\, X(\omega)$$

A typical plot of $|Z(\omega)|$, $\angle\theta(\omega)$, $R(\omega)$ and $X(\omega)$ is shown in Fig. 5.

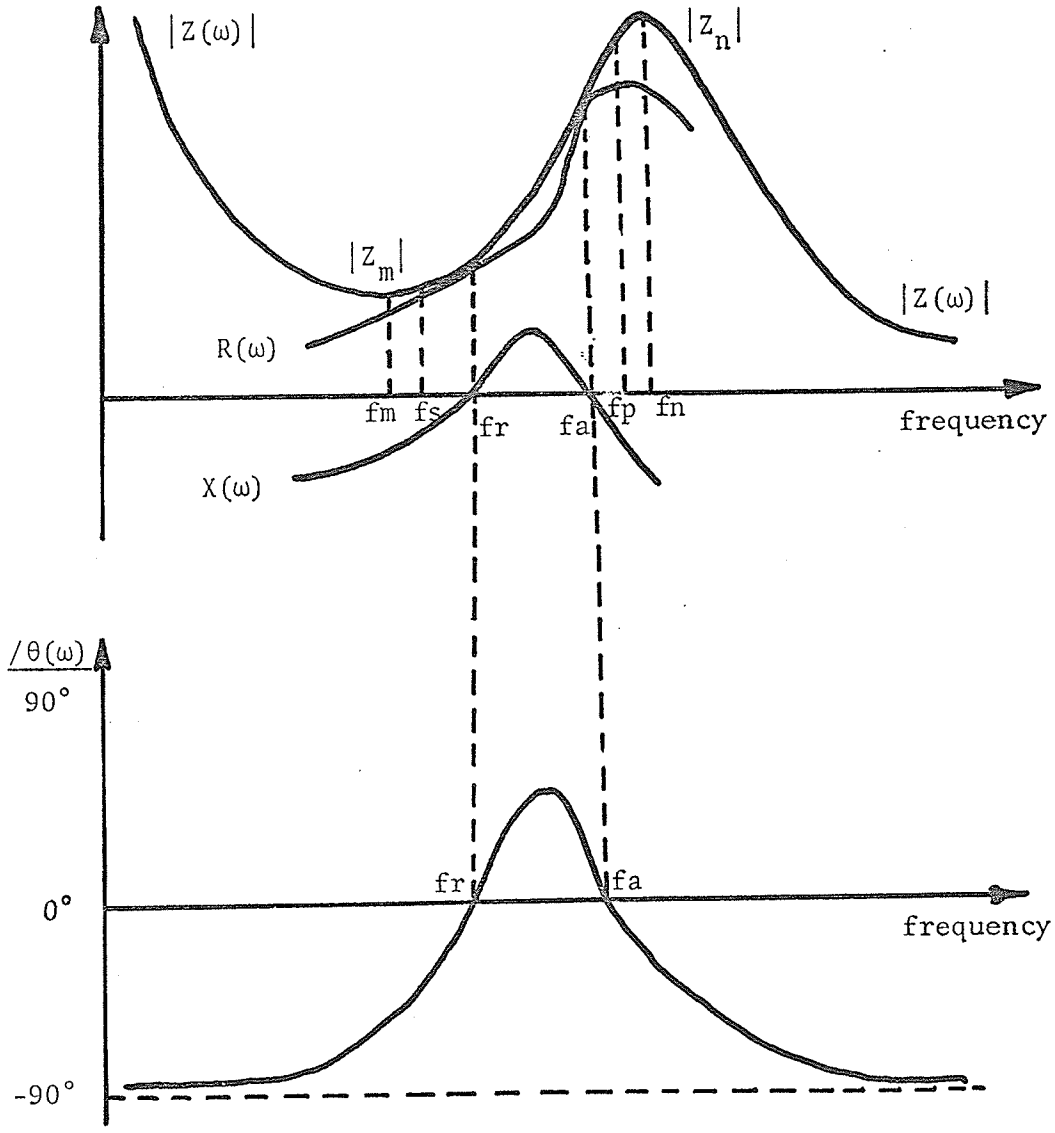

Fig. 5. Typical plot of $|Z(\omega)|$, $\angle\theta(\omega)$, $R(\omega)$ and $X(\omega)$ versus frequency.

The plot of $|Z(\omega)|$ shows a minimum value $|Z_m|$ at the frequency f_m and a maximum value $|Z_n|$ at f_n. There are two frequencies f_r and f_a at which the impedance is purely resistive. From equation (1), we expect that f_s lies between f_m and f_r, and f_p lies between f_a and f_n.

From an experimental view, it is rather difficult to measure f_s and f_p. However, since f_m, f_r, f_a and f_n are easily determined, a technique is used to derive the parameters R, L, C and C_o of the electrical circuit from the knowledge of f_m, f_r, f_a, f_n, $|Z_m|$ and $|Z_n|$.

At this point, we note that the method is only valid for a transducer with an impedance which exhibits the approximate behaviour of the curves shown in Fig. 5; in particular, the plot of $|Z(\omega)|$ should exhibit one minimum and one maximum like the one shown in Fig. 5. Hence a plot of the input impedance as a function of the frequency is necessary to guarantee the applicability of the method.

B. Determination of the parameters

Putting $Q_1 = Q\sqrt{\frac{1+r}{r}}$ and $K = \frac{\omega_s RQ}{r}$ in Eq. (1) and taking the absolute value of the impedance, we get

$$|Z(\omega)| = \frac{K}{\omega}\frac{\sqrt{1 + Q^2\left(\frac{\omega}{\omega_s} - \frac{\omega_s}{\omega}\right)^2}}{\sqrt{1 + Q_1^2\left(\frac{\omega}{\omega_p} - \frac{\omega_p}{\omega}\right)^2}} \qquad (2)$$

and

$$|Z(\omega)|^2 = \frac{K^2}{\omega^2} \frac{1 + Q^2 \left\{ \frac{\omega^2}{\omega_s^2} + \frac{\omega_s^2}{\omega^2} - 2 \right\}}{1 + Q_1^2 \left\{ \frac{\omega^2}{\omega_p^2} + \frac{\omega_p^2}{\omega^2} - 2 \right\}}$$

$$|Z(\omega)|^2 = \frac{K^2 + \omega^2 \frac{K^2 Q^2}{\omega_s^2} + \frac{\omega_s^2 K^2 Q^2}{\omega^2} - 2Q^2 K^2}{\omega^2 + \frac{\omega^4 Q_1^2}{\omega_p^2} + \omega_p^2 Q_1^2 - 2\omega^2 Q_1^2} \qquad (3)$$

By multiplying through by the denominator of the right hand side and by using $k = \sqrt{\frac{1 + r}{r}}$ and $\frac{\omega_s RQ}{r} = K$, we have after grouping and factoring:

$$\left\{ |Z(\omega)|^2 \omega^6 \frac{k^2}{\omega_p^2} + |Z(\omega)|^2 \omega^2 \omega_p^2 k^2 - 2|Z(\omega)|^2 \omega^4 k^2 \right\} Q^2$$

$$- \left\{ \omega^2 \frac{\omega_s^2}{r^2} \right\} R^2 Q^2 + \left\{ 2\omega^2 \frac{\omega_s^2}{r^2} - \frac{\omega^4}{r^2} - \frac{\omega_s^4}{r^2} \right\} R^2 Q^4 = - |Z(\omega)|^2 \omega^4 \qquad (4)$$

By letting $X = Q^2$ and $Y = R^2$, Eq. (4) will have the form

$$AX - BXY + CX^2Y = D \qquad (5)$$

where

$$A = |Z(\omega)|^2 \omega^2 k^2 \left[\frac{\omega^4}{\omega_p^2} + \omega_p^2 - 2\omega^2 \right]$$

$$B = \frac{\omega^2 \omega_s^2}{r^2}$$

$$C = \frac{1}{r^2} \left[2\omega^2 \omega_s^2 - \omega^4 - \omega_s^4 \right]$$

$$D = - |Z(\omega)|^2 \omega^4$$

We note that

$$\frac{\omega_p}{\omega_s} = \frac{f_p}{f_s} = \frac{\frac{1}{2\pi LC}\sqrt{\frac{r+1}{r}}}{\frac{1}{2\pi\sqrt{LC}}} = \sqrt{\frac{r+1}{r}} = k \qquad (6)$$

Thus

$$r = \frac{1}{k^2 - 1} = \frac{1}{\left(\frac{f_p}{f_s}\right)^2 - 1} \qquad (7)$$

Therefore A, B, C and D are function of $|Z(\omega)|$, f_p, f_s and ω. Suppose we know f_p, f_s and two pair of values $(|Z(\omega_1)|, \omega_1)$ and $(|Z(\omega_2), \omega_2|)$, we then get two equations in two unknowns, X and Y

$$A(f_p, f_s, |Z(\omega_1)|, \omega_1)X - B(f_p, f_s, |Z(\omega_1)|, \omega_1)XY + C(f_p, f_s, |Z(\omega_1)|, \omega_1)X^2 Y$$

$$= D(f_p, f_s, |Z(\omega_1)|, \omega_1)$$

$$A(f_p, f_s, |Z(\omega_2)|, \omega_2)X - B(f_p, f_s, |Z(\omega_2)|, \omega_2)XY + C(f_p, f_s, |Z(\omega_2)|, \omega_2)XY^2$$

$$= D(f_p, f_s, |Z(\omega_2)|, \omega_2)$$

or simply:

$$A_1X - B_1XY + C_1X^2Y = D_1 \tag{8}$$

$$A_2X - B_2XY + C_2X^2Y = D_2 \tag{9}$$

From (8) we have:

$$Y = \frac{D_1 - A_1X}{X(C_1X - B_1)} \tag{10}$$

Substituting (10) in (9):

$$A_2X - B_2X\,\frac{D_1 - A_1X}{X(C_1X - B_1)} + C_2X^2\,\frac{D_1 - A_1X}{X(C_1X - B_1)} = D_2$$

or

$$(A_2C_1 - A_1C_2)X^2 - (A_2B_1 - A_1B_2 + C_1D_2 - C_2D_1)X + (B_1D_2 - B_2D_1) = 0 \tag{11}$$

We recognize (11) as a quadratic equation of the form:

$mx^2 - px + q = 0$. The solutions of which are given by:

$$X = \frac{p \pm \sqrt{p^2 - 4mq}}{2m}$$

Since X is equal to Q^2, we must select the positive solution

$$Q = + \sqrt{X} \qquad \text{with} \qquad X > 0 \tag{12}$$

By substituting the same solution in (10):

$$R = + \sqrt{Y} \qquad \text{with} \qquad Y > 0 \tag{13}$$

From the definition of the quality factor Q, we get

$$L = \frac{Q.R}{2\pi f_s} = \frac{Q.R}{\omega_s} \tag{14}$$

Thus

$$C = \frac{1}{L\ \omega_s^2} \tag{15}$$

and finally

$$C_o = rC \tag{16}$$

We need to know f_s, f_p and two pairs of values $(|Z(\omega_1)|, \omega_1)$ and $(|Z(\omega_2)|, \omega_2)$ in order to obtain Eq. (8) and Eq. (9). The procedure used to find the four parameters of the equivalent circuit is then a cut-and-try technique, the steps of which are given below:

1. We obtain an experimental plot of the impedance of the transducer as a function of the frequency by using an impedance meter.
2. From the experimental curve, we select the characteristic values f_m, f_r, f_a, f_n, $|Z_m|$ and $|Z_n|$.
3. We choose a pair of values (f_s, f_p) such that:

   $f_m \leq f_s \leq f_r$ and $f_a \leq f_p \leq f_n$

   The chosen pair (f_s, f_p) and the two pairs of values $(|Z_m|, f_m)$ and $(|Z_n|, f_n)$ determine the coefficients of the equations (8) and (9) from which we can solve for a possible set of parameters R, L, C and C_o.

4. From this possible set of parameters, we plot the corresponding fitting impedance curve.
5. We repeat steps 3 and 4 with another pair (f_s, f_p).
6. The selection of an acceptable fitting impedance curve is based on the following criteria.

C. Criteria for the selection of an acceptable curve

First, we attempt to calculate the relative error of the parameters. From the expression (1), we can write the absolute value:

$$|Z(\omega)| = \frac{\omega_s RQ}{\omega r} \frac{\sqrt{1 + Q^2 \left(\frac{\omega}{\omega_s} - \frac{\omega_s}{\omega}\right)^2}}{\sqrt{1 + Q^2 \left(\frac{1 + r}{r}\right)\left(\frac{\omega}{\omega_p} - \frac{\omega_p}{\omega}\right)^2}} \tag{17}$$

At $\omega = \omega_s$ we have

$$|Z(\omega_s)| = \frac{RQ}{r} \frac{1}{\sqrt{1 + Q^2\left(\frac{1 + r}{r}\right)\left(\frac{\omega_s}{\omega_p} - \frac{\omega_p}{\omega_s}\right)^2}} \tag{18}$$

If $$Q^2\left(\frac{1 + r}{r}\right)\left(\frac{\omega_s}{\omega_p} - \frac{\omega_p}{\omega_s}\right)^2 \gg 1 \tag{19}$$

then

$$|Z(\omega_s)| \simeq \frac{RQ}{rQ\sqrt{\left(\frac{1 + r}{r}\right)}\left(\frac{\omega_s}{\omega_p} - \frac{\omega_p}{\omega_s}\right)} = \frac{R}{\sqrt{r(1 + r)}\left(\frac{\omega_s}{\omega_p} - \frac{\omega_p}{\omega_s}\right)} \tag{20}$$

Replacing r by its equivalent (cf.(7)) we get:

$$|Z(\omega_s)| \simeq R \tag{21}$$

Hence $$\left| \frac{\Delta|Z(\omega_s)|}{|Z(\omega_s)|} \right| = \left| \frac{\Delta R}{R} \right| \tag{22}$$

At $\omega = \omega_p$:

$$|Z(\omega_p)| = \frac{\omega_s}{\omega_p} \frac{RQ}{r} \sqrt{1 + Q^2 (\frac{\omega_p}{\omega_s} - \frac{\omega_s}{\omega_p})^2} \tag{23}$$

If $$Q^2 (\frac{\omega_p}{\omega_s} - \frac{\omega_s}{\omega_p})^2 >> 1 \tag{24}$$

(Note that (19) is satisfied if (24) is satisfied and that both are normally met) Then

$$|Z(\omega_p)| \simeq \frac{\omega_s}{\omega_p} \frac{RQ^2}{r} (\frac{\omega_p}{\omega_s} - \frac{\omega_s}{\omega_p}) = RQ^2 \left[\frac{\omega_p^2 - \omega_s^2}{\omega_p \omega_s} \right]^2$$

and

$$Q^2 \simeq \frac{|Z(\omega_p)|}{R} \cdot \left[\frac{f_p f_s}{f_p^2 - f_d^2} \right]^2 \tag{25}$$

If we assume that the exact values of f_p and f_s are known then the maximum relative error of Q is

$$\left| \frac{\Delta Q}{Q} \right| = \frac{1}{2} \left\{ \left| \frac{\Delta|Z(\omega_p)|}{|Z(\omega_p)|} \right| + \left| \frac{\Delta R}{R} \right| \right\} = \frac{1}{2} \left\{ \left| \frac{\Delta|Z(\omega_p)|}{|Z(\omega_p)|} \right| + \left| \frac{\Delta|Z(\omega_s)|}{|Z(\omega_s)|} \right| \right\} \tag{26}$$

From (14) we calculate the relative error of L:

$$\left|\frac{\Delta L}{L}\right| = \left|\frac{\Delta Q}{Q}\right| + \left|\frac{\Delta R}{R}\right| = \frac{3}{2}\left|\frac{\Delta|Z(\omega_s)|}{|Z(\omega_s)|}\right| + \frac{1}{2}\left|\frac{\Delta|Z(\omega_p)|}{|Z(\omega_p)|}\right| \tag{27}$$

From (15) and (16):

$$\left|\frac{\Delta C}{C}\right| = \left|\frac{\Delta C_o}{C_o}\right| = \left|\frac{\Delta L}{L}\right| \tag{28}$$

The relative error of C and C_o may be calculated in another way independent of the conditions (19) and (24). We notice that at very low frequencies, the electric model behaves like C and C_o in parallel because R is negligible with respect to the reactance $\frac{1}{C\omega_\ell}$; whereas at high frequencies, it behaves like C_o (Fig. 6 and Fig. 7):

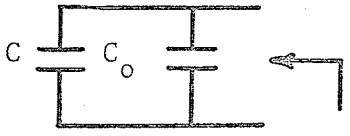

$$|Z(\omega_\ell)| = \frac{1}{(C_o + C)\omega_\ell} = \frac{1}{(r+1)C\omega_\ell}$$

Fig. 6. Electrical Model at low frequency.

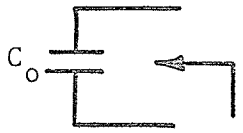

$$|Z(\omega_h)| = \frac{1}{C_o\omega_h}$$

Fig. 7. Electrical Model at high frequency.

From these considerations we have

$$\left|\frac{\Delta C}{C}\right| = \left|\frac{\Delta C_o}{C_o}\right| = \left|\frac{\Delta|Z(\omega_\ell)|}{|Z(\omega_\ell)|}\right| = \left|\frac{\Delta|Z(\omega_h)|}{|Z(\omega_\ell)|}\right| \tag{29}$$

From this study of relative error, we point out certain critical regions of the impedance curve which would determine the error; they are shown in heavy lines in Fig. 8. Regions I and II are critical because the exact values of f_s and f_p, which are assumeed to be known, lie in these regions.

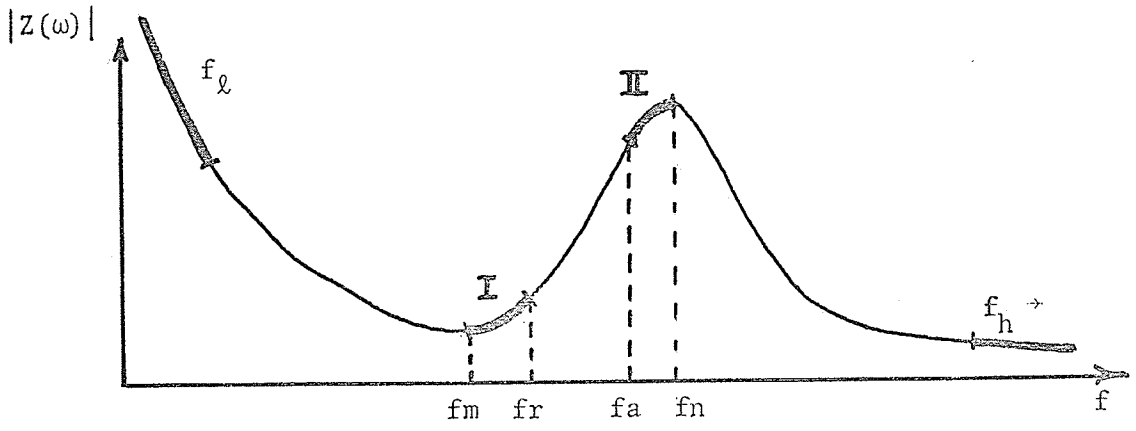

Fig. 8. Critical regions of the theoretical curve $|Z(\omega)|$

An acceptable fitting curve must fit as closely as possible in these critical regions. If the tolerance $\left.\frac{\Delta Z}{Z}\right|_{FE}$ of the fitting curve is chosen to be a fraction $\lambda < 1$ of the experimental tolerance then the overall tolerance is

$$\left|\frac{\Delta|Z(\omega)|}{|Z(\omega)|}\right| = (\lambda + 1)\left|\frac{\Delta|Z(\omega)|}{|Z(\omega)|}\right|_{\text{experimental}} \tag{30}$$

If (30) is satisfied, then the relative error of the acceptable para-

meters R, L, C and C_o are given by (22), (27), (28) and (29).

However, the behavior of the experimental curve may deviate from the fitting curve outside those critical regions. We distinguish two cases:

1. The transducer may have other modes of resonance outside the region of resonance. If these resonances are of minor importance, i.e., they occur outside the band of frequency of interest or if the magnitude of the corresponding peak is relatively small compared with the peak of the main resonance, the fitting curve is still satisfactory. An acceptable deviation is shown in Fig. 9.

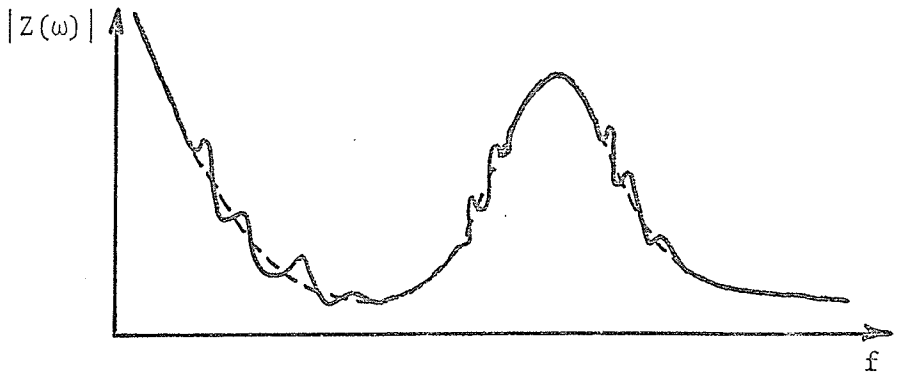

Fig. 9. An acceptable deviation; the experimental curve shown in solid line and the fitting curve shown in dotted line.

2. The transducer may have a strong mode of resonance either outside the critical regions or near the region of resonance. In that case, the proposed electrical model is no longer valid as was pointed out earlier. An unacceptable deviation is shown in Fig. 10.

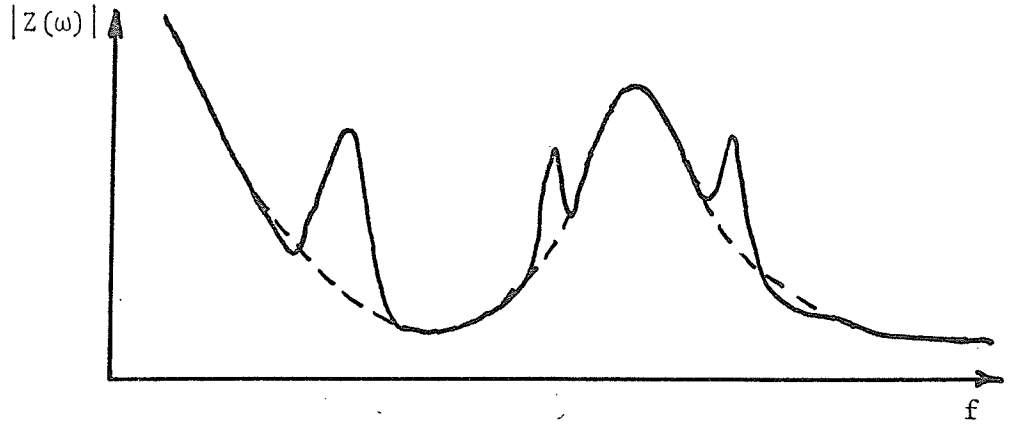

Fig. 10. An unacceptable deviation:
experimental curve shown in solid lines,
fitting curve shown in dotted lines.

Thus, a visual inspection of the impedance curve is necessary. Two or more experimental curves are said to be identical if they fall within the limit of tolerance (30) over the critical regions and satisfy the conditions of the first case; they are identical in the sense that an acceptable fitting curve of one of them would give the same electrical model to these curves.

So far, we have not discussed the relative error of f_s and f_p. Since they lie respectively in the interval (f_m, f_r) and (f_a, f_n). Let us divide these intervals into p and q subintervals. From the chosen p and q, we may assign arbitrary fixed frequency errors Δf_s and Δf_p to f_s and f_p. Here the use of the computer is advantageous due to the number of repetitions of steps 3 and 4 which is equal to the product pq. Since the pair (f_s, f_p) is chosen such that

$$f_m \leq f_s = f_m + m\,\Delta f_s \leq f_r \quad \text{with} \quad m = 0, 1, \ldots, p$$

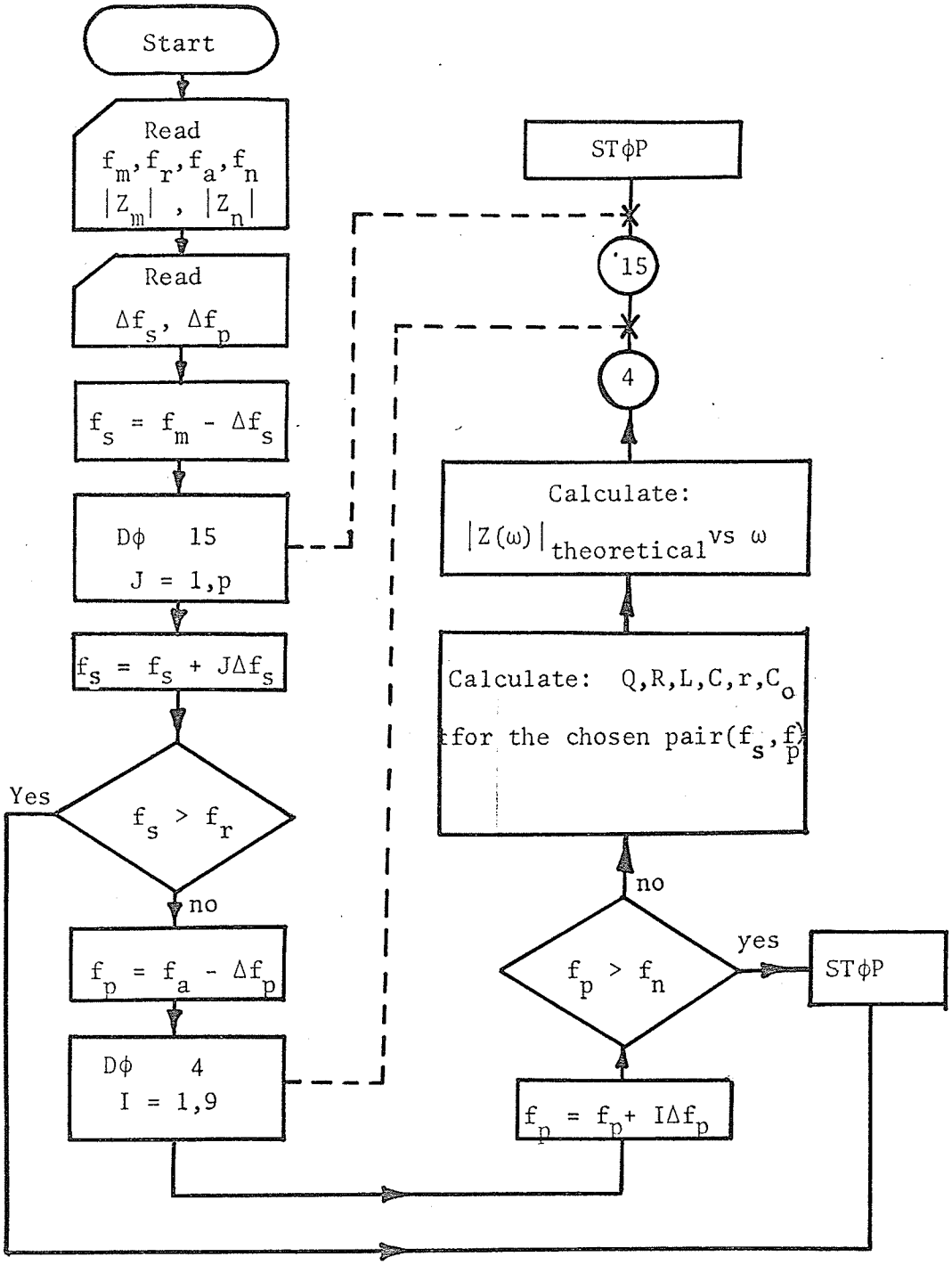

Fig. 11: Flow-chart of the computer program used in the fitting technique.

$$f_a \leq f_p = f_a + n\,\Delta f_p \leq f_n \qquad \text{with} \qquad n = 0, 1, \ldots, q$$

A computer flow-chart for steps 3 and 4 is shown in Fig. 11. From these plots, the proposed criteria will help to sort out an acceptable fitting curve which determines the electrical model.

D. Illustrative example

First, we attempt to find the electrical model of the unloaded transducer shown in Fig. 12. Such a transducer is used subsequently in the system shown in Fig. 1 for the study of acoustic emission from materials under stress in the range of frequency from 100 KHz to 300 KHz.

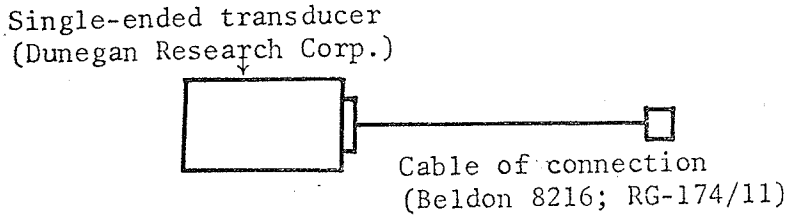

Fig. 12. Unloaded transducer with connection cable.

To measure the impedance of the transducer, we used the set up shown in Fig. 13. From the plot (Graph I), we recognize a minor resonance at 153 KHz. However it is an acceptable deviation and the method is applicable.

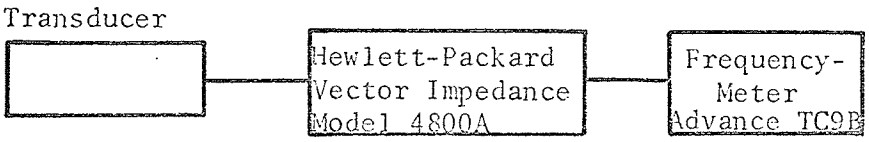

Fig. 13. Set up for the impedance measurement.

The characteristic values obtained from the impedance measurement are:

f_m = 129.4 KHz ; $|Z_m|$ = 796Ω

f_r = 129.7 KHz

f_a = 144.7 KHz

f_n = 145.7 KHz ; $|Z_n|$ = 15.2KΩ

The accuracy of the Vector impedance meter is ±5% for the measured impedance. The frequency is measured with the Advance timer counter the accuracy of which depends on the drift of the interval oscillator of the impedance meter. However, the accuracy may be estimated to ±0.1 KHz.

Hence we must fit our theoretical curve within ±5% over the critical regions of the experimental curve. Following the steps 3 and 4 and setting $\Delta f_s = \Delta f_p$ = 0.1 KHz, we found an acceptable curve (Graph I) with:

f_s = 129.5 KHz

f_p = 145.0 KHz

These values, together with the four above ($|Z_m|$, $|Z_n|$, f_m, f_n) give the set of acceptable values:

R = 817 ohms

Q = 18.15

L = 18.3 mH

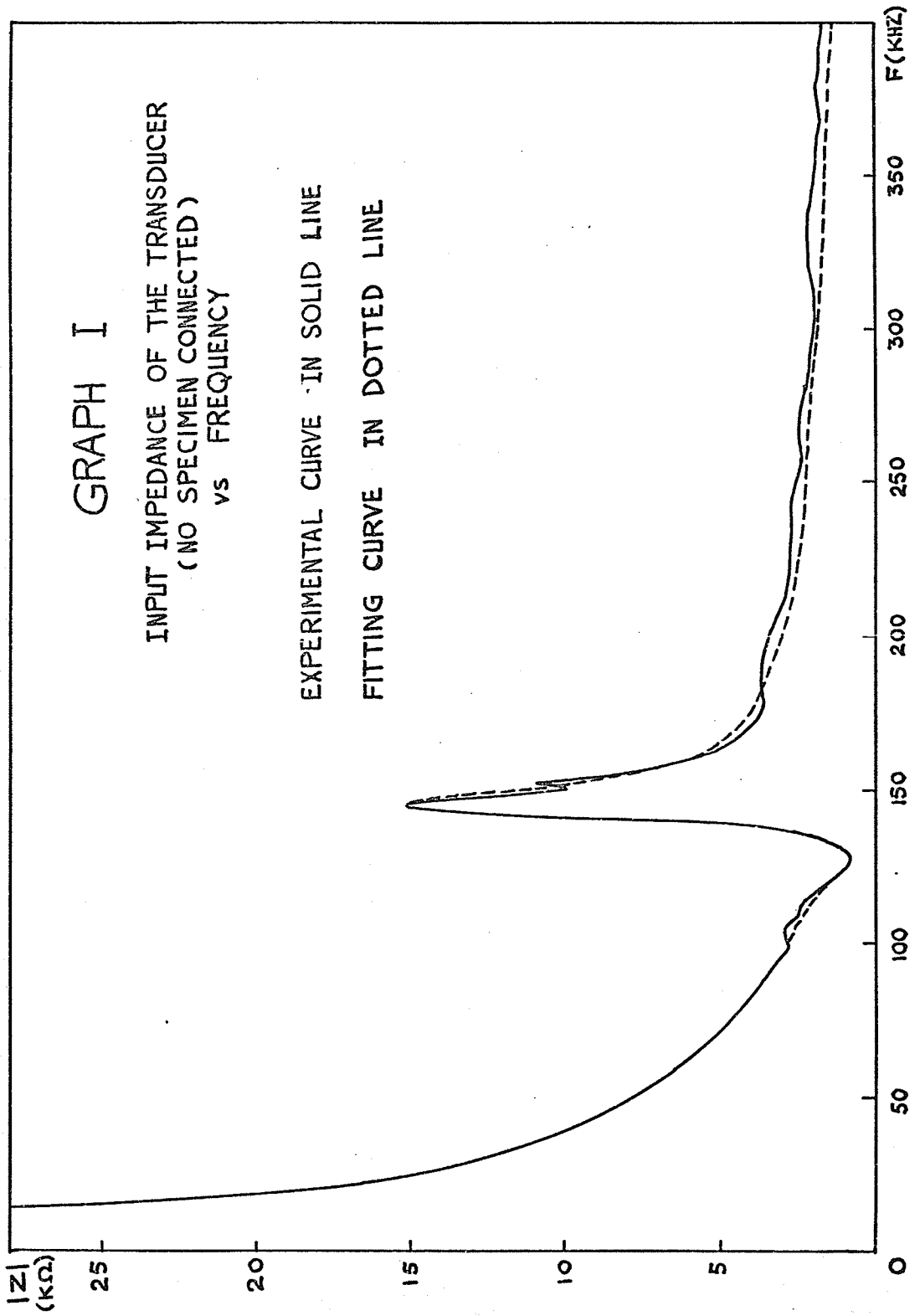
GRAPH I
INPUT IMPEDANCE OF THE TRANSDUCER
(NO SPECIMEN CONNECTED)
vs FREQUENCY
EXPERIMENTAL CURVE IN SOLID LINE
FITTING CURVE IN DOTTED LINE
|Z| (KΩ)
25
20
15
10
5
0
50
100
150
200
250
300
350
F(KHZ)

$C = 83$ pF

$C_o = 315$ pF

$\left.\frac{\Delta Z}{Z}\right|_{FE} = 3\%$

Let us check the condition stated in (24), we have:

$$Q^2\left(\frac{\omega_p}{\omega_s} - \frac{\omega_s}{\omega_p}\right)^2 = (18.15)^2\left(\frac{145}{129.5} - \frac{129.5}{145}\right)^2 = 17.7 \gg 1$$

Therefore from (22), (27) and (28)

$$\left|\frac{\Delta R}{R}\right| = \left|\frac{\Delta|Z|}{|Z|}\right| = 8\%$$

$$\left|\frac{\Delta L}{L}\right| = \frac{3}{2}\left|\frac{\Delta|Z|}{|Z|}\right| + \frac{1}{2}\left|\frac{\Delta|Z|}{|Z|}\right| = 16\%$$

$$\left|\frac{\Delta C}{C}\right| = \left|\frac{\Delta C_o}{C_o}\right| = \left|\frac{\Delta L}{L}\right| = 16\%$$

It is understood that the parameters must be time-invariant; that is, the impedance curve must be strictly identical independent of the time we start the measurement. By strictly identical we mean that the curves fall within the experimental error throughout the frequency range. This condition was satisfied by the measurement data.

For Fe 3% Si specimens connected to the transducer as shown in Fig. 14, the measurement of the impedance permits us to conclude that:

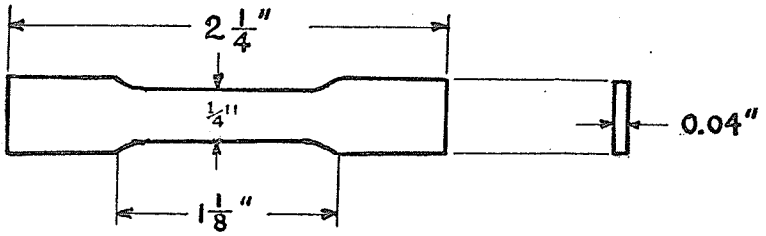

Fig. 14. Dimensions of the fe 3% Si Specimen.

1. The impedance curve is time-invariant.
2. The impedance curve is strictly identical if we mount specimens of the same size and of the same material on the transducer.
3. The impedance curve is strictly identical whether we do or do not mount the transducer and the specimen on the testing machine.
4. The impedance curve of the specimen is strictly identical before and after the test.
5. The impedance may not be identical according to the position of the specimen with respect to the rubber shoe of the transducer.
6. The impedance may not be identical for different amounts of the coupling fluid applied on the rubber shoe of the transducer.

The first conclusion is necessary as discussed earlier. The second conclusion may be drawn intuitively since all things are equal, except some slight difference in the preparation of the specimen, we must have the same curve. Similarly, the fourth conclusion follows since the strain rate is very small. The third one implies implicitly that the

transducer is clamped by the specimen. Therefore, mounting the specimen on the testing machine does not make any difference in the impedance measurement. The intrusion of the specimen hence reduces the effective mass of vibration of the transducer. Thus the inductance L decreases and we expect a higher resonant frequency. Conclusion 5 and 6 suggest that a small amount of coupling fluid be used and that the transducer should be in a fixed position with respect to the specimen.

The characteristic values from the impedance measurement (Graph II) are:

f_m = 132.7 KHz $\qquad |Z_m|$ = 900 ohms

f_r = 137.6 KHz

f_a = 154.1 KHz

f_n = 157.7 KHz $\qquad |Z_n|$ = 12.7 K ohms

Following steps 3 and 4 and setting $\Delta f_s = \Delta f_p$ = 0.5 KHz we found an acceptable curve (Graph II) with

f_s = 134.2 KHz

f_p = 155.1 KHz

these values together with the four above (f_m, $|Z_m|$, f_n, $|Z_n|$) give the set of parameters:

R = 948 ohms

Q = 12.3

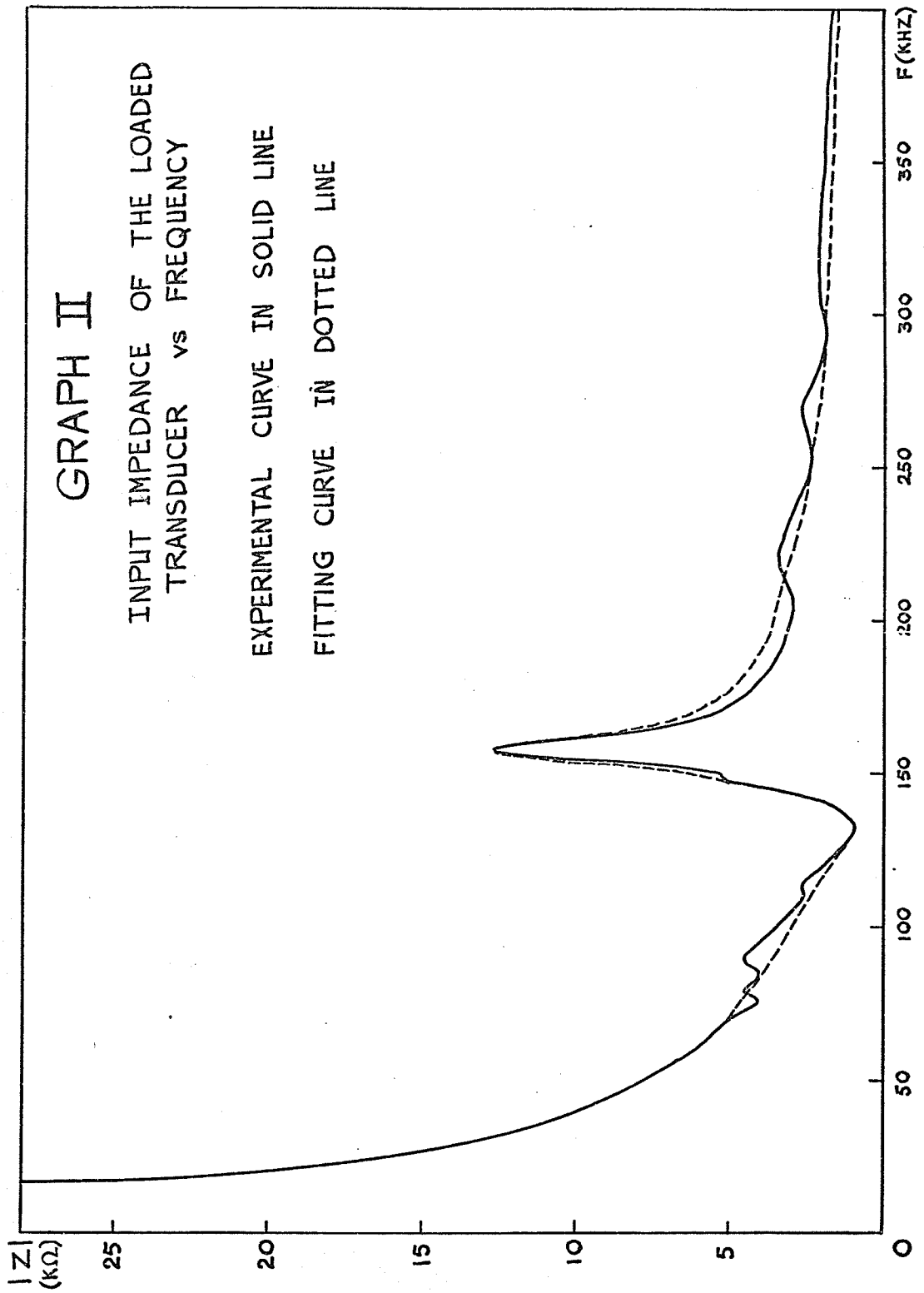
GRAPH II
INPUT IMPEDANCE OF THE LOADED TRANSDUCER vs FREQUENCY
EXPERIMENTAL CURVE IN SOLID LINE
FITTING CURVE IN DOTTED LINE
|Z| (KΩ)
25
20
15
10
5
0
50
100
150
200
250
300
350
F(KHZ)

$L = 13.8$ mH

$C = 102$ pF

$C_o = 302$ pF

$\left.\frac{\Delta Z}{Z}\right|_{FE} = 3\%$

We now check the condition stated in (24):

$$Q^2 \left(\frac{\omega_p}{\omega_s} - \frac{\omega_s}{\omega_p}\right)^2 = (12.3)^2 \left[\frac{155}{134} - \frac{134}{155}\right]^2 = 12.7 \gg 1$$

therefore from (22), (27) and (28):

$$\left|\frac{\Delta R}{R}\right| = \left|\frac{\Delta|Z|}{|Z|}\right| = 8\%$$

$$\left|\frac{\Delta L}{L}\right| = 2\left|\frac{\Delta|Z|}{|Z|}\right| = 16\%$$

$$\left|\frac{\Delta C}{C}\right| = \left|\frac{\Delta C_o}{C_o}\right| = \left|\frac{\Delta L}{L}\right| = 16\%$$

Up to this point, the sytem shown in Fig. 1 can be represented by Fig. 15:

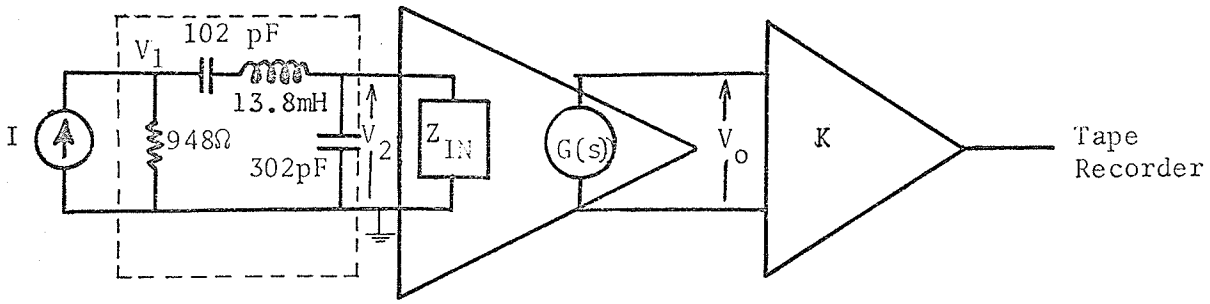

Fig. 15 Electrical model of the system shown in Fig. 1.

Where

I is the electrical analog of the mechanical force or of the acoustical pressure.

V_1 is the electrical analog of the velocity

V_2 is the electrical voltage at the output of the transducer

Z_{IN} is the input impedance of the preamplifier

G(s) is the transfer function of the preamplifier

V_o is the voltage at the output of the preamplifier

K is the gain of the wide-band amplifier

In the following chapter, we will calculate the impulse response of this system by first finding the transfer function:

$$Z_{21}(s) = \frac{V_2(s)}{I(s)}, \tag{31}$$

taking into account the possible loading effect of Z_{IN}, and then the overall transfer function:

$$T(s) = \frac{V_o(s)}{I(s)} = \frac{V_2(s)}{I(s)} \cdot \frac{V_o(s)}{V_2(s)} = Z_{21}(s)\ G(s) \tag{32}$$

We note that the voltage fed to the tape recorder is an amplified version of V_o. Finally we will consider applications which one may derive from the impulse response.

CHAPTER III

IMPULSE RESPONSE OF THE SYSTEM AND ITS APPLICATIONS

A. *Transfer function of the electrical model*

For the model connected to the preamplifier, we have the following circuit (Fig. 16):

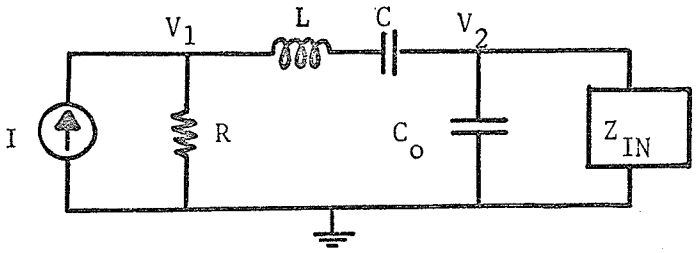

Fig. 16. Circuit used in the calculation of $Z_{21}(s)$, taking into account the loading effect of Z_{IN}

Using the node analysis method, we can write in the frequency domain:

$$\begin{bmatrix} I(s) \\ 0 \end{bmatrix} = \begin{bmatrix} G + Y & -Y \\ -Y & Y + Y_o \end{bmatrix} \begin{bmatrix} V_1(s) \\ V_2(s) \end{bmatrix}$$

where $G = \frac{1}{R}$; $\quad Y = \frac{1}{Ls + \frac{1}{Cs}} = \frac{Cs}{LCs^2 + 1}$

$$Y_o = C_o s + G_o \quad ; \quad G_o = \frac{1}{Z_{IN}}$$

Solving for $V_1(s)$ and $V_2(s)$, we obtain

$$\frac{V_2}{I} = \frac{Y}{GY + GY_o + YY_o} \tag{33}$$

$$\frac{V_1}{I} = \frac{Y + Y_o}{GY + GY_o + YY_o} \tag{34}$$

(33) and (34) can be written explicitly:

$$Z_{21}(s) = \frac{V_2(s)}{I(s)} = \frac{Cs}{A_3s^3 + A_2s^2 + A_1s + A_o} \tag{35}$$

$$\frac{V_1(s)}{I(s)} = R + \frac{B_2s^2 + B_1s + B_o}{A_3s^3 + A_2s^2 + A_1s + A_o} \tag{36}$$

where:

$$A_3 = LGCC_o \quad ; \qquad A_2 = LCGG_o + C_oC$$

$$A_1 = GC_o + GC + G_oC \; ; \quad A_o = GG_0$$

$$B_2 = -RCC_o \quad ; \qquad B_1 = -RG_oC \; ; \quad B_o = 0$$

We consider the following cases:

1. <u>The input impedance of the preamplifier is very large</u>.

This statement is essentially equivalent to saying that $G_o = 0$

Then

$$\frac{V_2}{I} = \frac{C}{(LGCC_o)s^2 + (C_oC)s + G(C + C_o)} \tag{37}$$

$$\frac{V_1}{I} = R\left[1 - \frac{C_oCs}{(LGCC_o)s^2 + (C_oC)s + G(C + C_o)}\right] \tag{38}$$

It is interesting to put (37) in the following form:

$$\frac{V_2}{I} = \frac{R}{LC_o} \cdot \frac{1}{[s + \zeta\omega_n]^2 + [\omega_n \sqrt{1 - \zeta^2}]^2} \tag{39}$$

where:

$$\zeta = \frac{R}{2} \sqrt{\frac{C_{eq}}{L}} \quad (40) \quad \text{with} \quad C_{eq} = \frac{CC_o}{C + C_o} \tag{41}$$

$$\omega_n = \frac{1}{\sqrt{LC_{eq}}} = \omega_p = \text{the parallel resonance angular frequency of the transducer} \tag{42}$$

(Note that ω_n here does not denote the angular frequency at which the impedance of the transducer is maximum)

ζ and ω_n are known respectively as the damping factor and the undamped frequency of oscillation of the second order system defined by (39).

Three other quantities are derived from ζ and ω_n [9], they are:

$$\omega_o = \omega_n \sqrt{1 - \zeta^2} \quad \text{(damped frequency of oscillation)} \tag{43}$$

$$Q = \frac{1}{2\zeta} \quad \text{(Figure of merit of the circuit)} \tag{44}$$

$$\omega_{max} = \omega_n \sqrt{1 - 2\zeta^2} \quad \text{(Frequency at which the transmission is maximum)} \tag{45}$$

The unit impulse response of the circuit can be found by setting $I(s) = 1$. Then

$$V_2(s) = \frac{R/LC_o}{(s + \zeta\omega_n)^2 + (\omega_n \sqrt{1 - \zeta^2})^2} \tag{46}$$

which corresponds in the time domain to

$$v_2(t) = \frac{R}{LC_o\omega_o} \exp(-\zeta\omega_n t) \sin(\omega_o t)\, u(t) \tag{47}$$

On the other hand,

$$V_1(s) = R\left[1 - \frac{R/L}{(s + \zeta\omega_n)^2 + (\omega_n\sqrt{1-\zeta^2})^2}\right] \tag{48}$$

which corresponds in the time domain to

$$v_1(t) = R\delta(t) - \frac{R^2}{L}\exp(-\zeta\omega_n t)\left[\cos\omega_o t - \zeta\frac{\omega_n}{\omega_o}\sin\omega_o t\right]u(t)$$

$$= R\delta(t) + \frac{R^2}{L}\sqrt{1+\zeta^2\frac{\omega_n^2}{\omega_o^2}}\exp(-\zeta\omega_n t)\sin(\omega_o t - \cot^{-1}\frac{\zeta\omega_n}{\omega_o})u(t)$$

where $u(t)$ is the unit step function. (49)

2. Transfer function of the model for $G_o = G(\omega)$

Actually, we found that the input impedance of the preamplifier is frequency dependent. The set up shown in Fig. 17 was used to measure the input impedance:

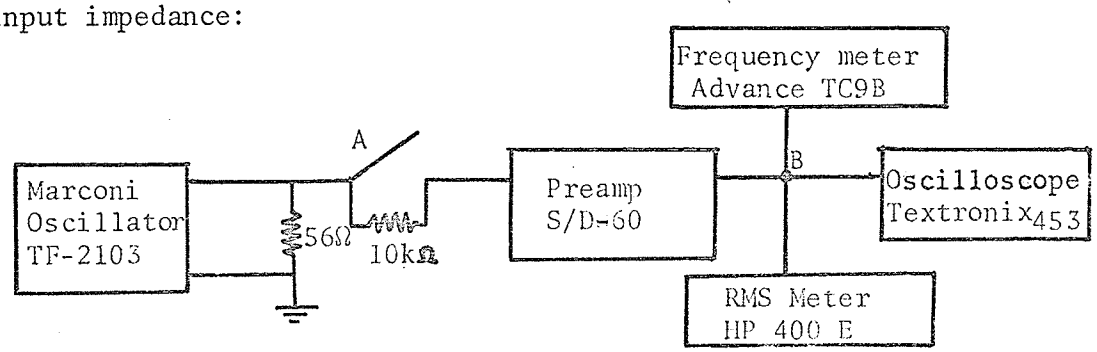

Fig. 17. Set up for the input impedance measurement.

The input impedance is given by:

$$Z_{IN} = 10\ K\Omega \cdot \frac{V_{2B}}{V_{1B} - V_{2B}} \tag{50}$$

where

V_{2B} is the measured voltage at B when the switch A is open, and

V_{1B} is the measured voltage at B when the switch A is closed.

A plot of Z_{IN} is given in Graph III.

Another plot of Z_{IN} where the magnitude is in dB is given in Graph IV.

Using Bode's design method [10] we obtain an approximate model for the input impedance:

$$Z^*_{IN} = 18.9\ K\Omega \left(\frac{\omega_1}{\omega_2}\right)^2 \frac{s^2 + 2\zeta_2\omega_2 s + \omega_2^2}{s^2 + 2\zeta_1\omega_1 s + \omega_1^2} \tag{51}$$

where

$$\omega_1 = 2\pi(150\ KHz) \quad ; \quad \zeta_1 = 0.45$$

$$\omega_2 = 2\pi(300\ KHz) \quad ; \quad \zeta_2 = 0.50$$

A plot of $|Z^*_{IN}|$ is given in Graph IV.

From (51) we can write

$$G_o = \frac{1}{Z^*_{IN}} = A \cdot \frac{s^2 + Ds + E}{s^2 + Ps + Q} \tag{52}$$

where $A = \frac{1}{18.9K\Omega} \cdot \left(\frac{\omega_2}{\omega_1}\right)^2$

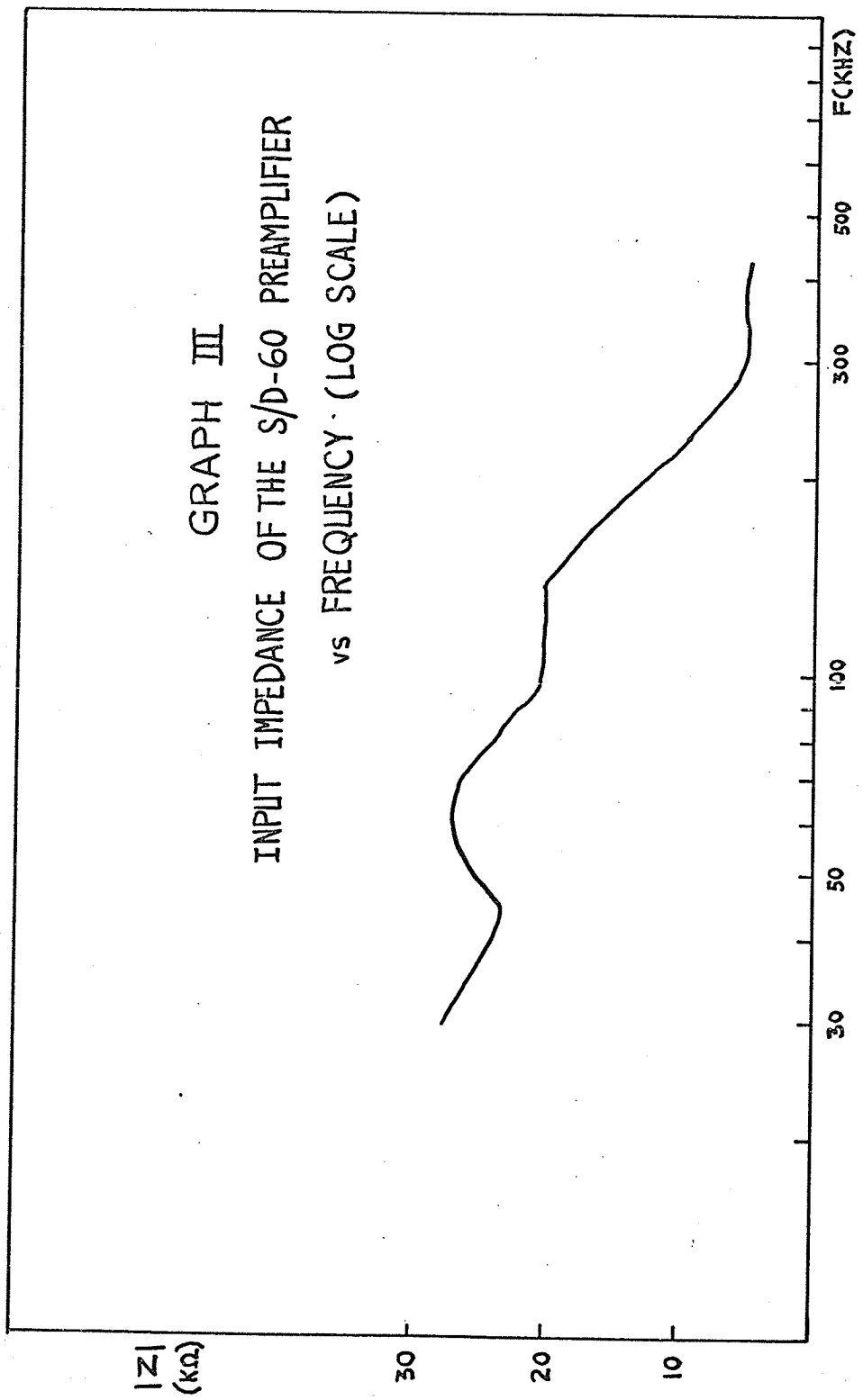
GRAPH III
INPUT IMPEDANCE OF THE S/D-60 PREAMPLIFIER
vs FREQUENCY (LOG SCALE)
|Z|
(KΩ)
30
20
10
30
50
100
300
500
F(KHZ)

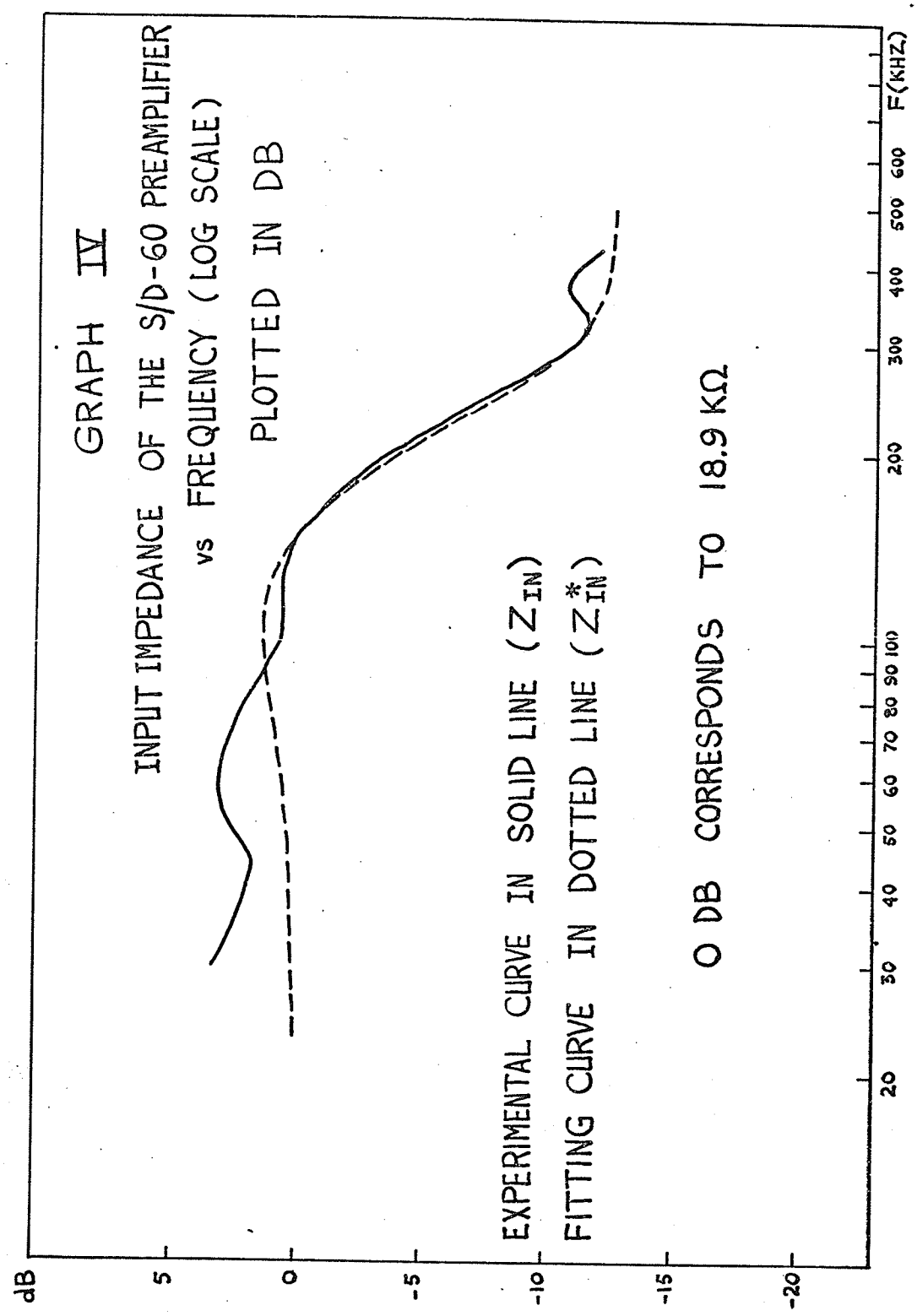
GRAPH IV
INPUT IMPEDANCE OF THE S/D-60 PREAMPLIFIER
vs FREQUENCY (LOG SCALE)
PLOTTED IN DB
dB
5
0
-5
-10
-15
-20
20
30
40
50
60
70
80
90
100
200
300
400
500
600
F(KHZ)
EXPERIMENTAL CURVE IN SOLID LINE (Z_{IN})
FITTING CURVE IN DOTTED LINE (Z^*_{IN})
O DB CORRESPONDS TO 18.9 KΩ

$$D = 2\zeta_1\omega_1 \qquad ; \qquad E = \omega_1^2$$

$$P = 2\zeta_2\omega_2 \qquad ; \qquad Q = \omega_2^2$$

Substituting (52) in (35) and (36), we get

$$Z_{21}(s) = \frac{V_2(s)}{I(s)} = \frac{Cs(s^2 + Ps + Q)}{H_5s^5 + H_4s^4 + H_3s^3 + H_2s^2 + H_1s + H_o} \tag{53}$$

$$\frac{V_1(s)}{I(s)} = R + \frac{F_4s^4 + F_3s^3 + F_2s^2 + F_1s + F_o}{H_5s^5 + H_4s^4 + H_3s^3 + H_2s^2 + H_1s + H_o} \tag{54}$$

where $H_5 = LGCC_o$

$H_4 = LGCC_oP + C_oC + LCGA$

$H_3 = LGCC_oQ + C_oCP + LCGAD + G(C + C_o) + CA$

$H_2 = C_oCQ + LCGAE + G(C + C_o)P + CAD + GA$

$H_1 = G(C + C_o)Q + CAE + GAD$

$H_o = GAE$

$F_4 = - RCC_o$

$F_3 = - RC(A + C_oP)$

$F_2 = - RC(C_oQ + AD)$

$F_1 = - RCAE$

$F_o = 0$

With the typical values in Fig. 15, we plot the transfer impedance $|Z_{21}(s)|$ for the three following cases on Graph V:

a) $G_o = 0$ (curve 1), i.e. with no loading effect

b) $G_o = G(\omega)$ (curve 2), using the experimental value of Z_{IN}

c) $G_o = \frac{1}{Z^*_{IN}}$ (curve 3), using the model for the input impedance Z_{IN}

using, respectively, expressions (37), (35) and (53). We notice that at high frequency, their behavior is identical; i.e.,

$$\frac{V_2}{I} \to \frac{R}{LC_o s^2} \qquad \text{as} \qquad s \to \infty$$

Graph V shows that in fact the three curves start to coincide from 500 KHz. On the other hand, curve 2 and curve 3 are within 2dB in the range 100 KHz to 300 KHz. This error is due the modeling used for the input impedance Z_{IN}. Obviously, we need a more elaborate model for better accuracy. However, for practical purpose, the model is judged satisfactory since the resulting impulse response will have only a slight error in the time domain.

Setting $I(s) = 1$, (53) and (54) can be written as

$$V_2(s) = \sum_{i=1}^{5} \frac{K_i}{s - s_i} \tag{55}$$

$$V_1(s) = R + \sum_{i=1}^{5} \frac{J_i}{s - s_i} \tag{56}$$

where

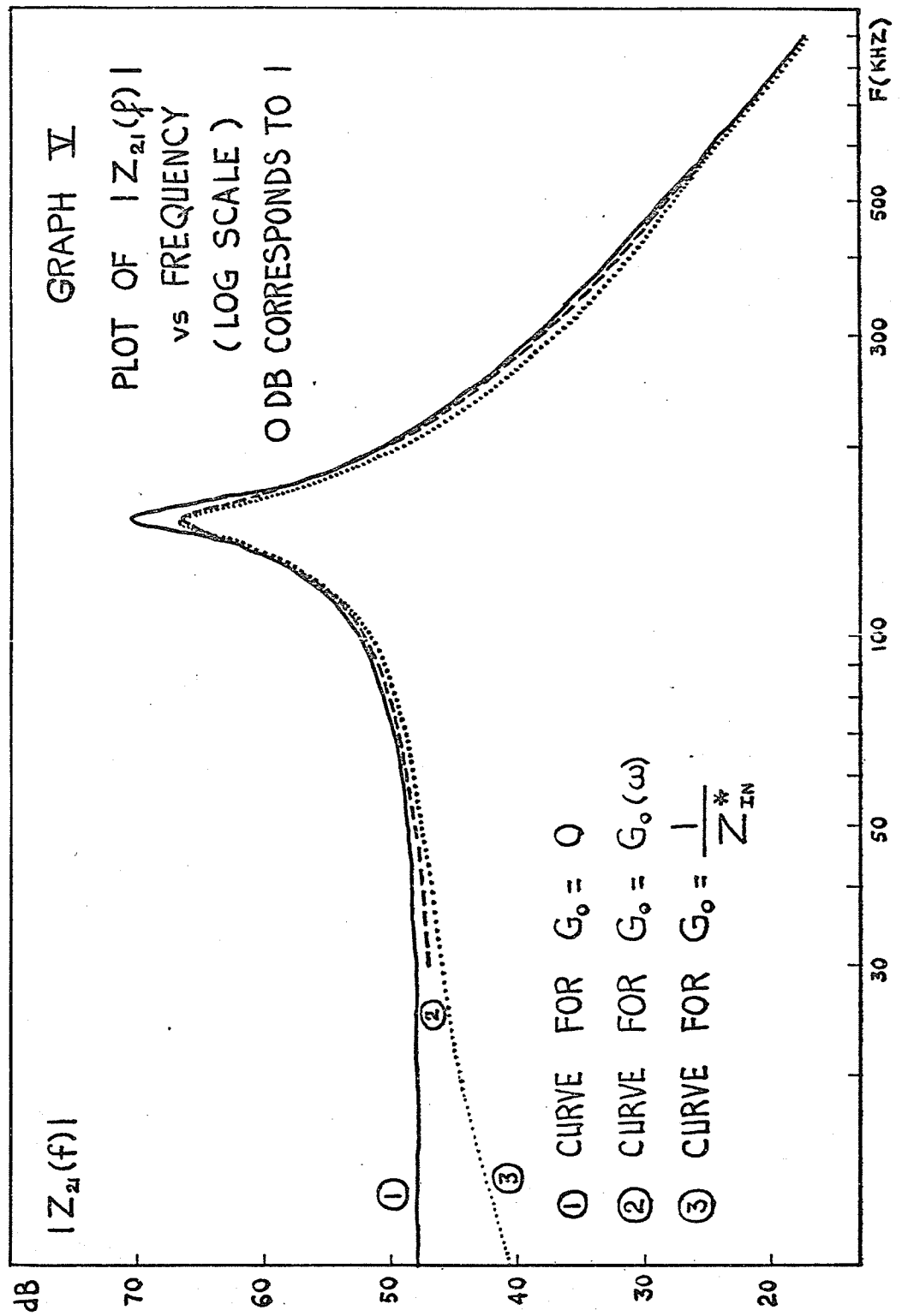
GRAPH V
PLOT OF $|Z_{21}(f)|$
vs FREQUENCY
(LOG SCALE)
O DB CORRESPONDS TO 1
$|Z_{21}(f)|$
dB
70
60
50
40
30
20
30
50
100
300
500
F(KHZ)
① CURVE FOR $G_0 = 0$
② CURVE FOR $G_0 = G_0(\omega)$
③ CURVE FOR $G_0 = \frac{1}{Z^*_{IN}}$

s_i are the roots of the polynomial $H_5s^5+H_4s^4+H_3s^3+H_2s^2+H_1s+H_o$,

K_i are the residues of (53) at the poles s_i and

J_i are the residues of the second term of (54) at the poles s_i.

In the time domain, we have

$$v_2(t) = \sum_{i=1}^{5} K_i e^{s_i t} \tag{57}$$

$$v_1(t) = R\delta(t) + \sum_{i=1}^{5} J_i e^{s_i t} \tag{58}$$

3. Numerical Applications

Using the model of Z_{IN} and the values for L, C, C_o and R, the roots of the polynomial

$$0.449 \times 10^{-24}s^5 + 0.119 \times 10^{-17}s^4 + 0.237 \times 10^{-11}s^3 + 0.143 \times 10^{-5}s^2 + 0.172 \times 10^{1}s + 0.198 \times 10^{6}$$

are found to be (using the IBM 360 computer)

$s_1 = -0.125 \times 10^6$

$s_2 = -0.429 \times 10^5 - j\ 0.956 \times 10^6$

$s_3 = \bar{s}_2$ (complex conjuguate of s_2)

$s_4 = -0.122 \times 10^7 - j\ 0.152 \times 10^7$

$s_5 = \bar{s}_4$

And the residues:

$$K_1 = -\ 0.291 \times 10^8$$

$$K_2 = 0.477 \times 10^7 + j\ 0.101 \times 10^9$$

$$K_3 = \bar{K}_2$$

$$K_4 = 0.980 \times 10^7 + j\ 0.177 \times 10^8$$

$$K_5 = \bar{K}_4$$

$$J_1 = 0.350 \times 10^6$$

$$J_2 = -\ 0.320 \times 10^8 + j\ 0.406 \times 10^6$$

$$J_3 = \bar{J}_2$$

$$J_4 = -\ 0.706 \times 10^6 - j\ 0.242 \times 10^6$$

$$J_5 = \bar{J}_4$$

Hence we have from (57) and (58):

$$v_2(t) = \Big\{ -0.291 \times 10^8 \exp(-0.125 \times 10^6 t) + 2 \exp(-0.429 \times 10^5 t) \times \Big[0.477 \times 10^7 \cos(0.956 \times 10^6 t) + 0.101 \times 10^9 \sin(0.956 \times 10^6 t) \Big] + 2 \exp(-0.122 \times 10^7 t) \times \Big[0.980 \times 10^7 \cos(0.152 \times 10^7 t) + 0.177 \times 10^8 \sin(0.152 \times 10^7 t) \Big] \Big\}\ u(t) \qquad (59)$$

And

$$v_1(t) = 948\,\delta(t) + \Big\{0.350 \times 10^6 \exp(-0.125 \times 10^6 t) + 2\exp(-0.429 \times 10^5 t) \times \Big[-0.320 \times 10^8 \cos(0.956 \times 10^6 t) + 0.406 \times 10^6 \sin(0.956 \times 10^6 t)\Big] + 2\exp\Big[-0.122 \times 10^7 t\Big] \times \Big[-0.706 \times 10^6 \cos(0.152 \times 10^7 t) - 0.242 \times 10^6 \sin(0.152 \times 10^7 t)\Big]\Big\}\, u(t) \qquad (60)$$

While from (40), (42), (43), (44), (45), (47) and (49):

$$\zeta = 0.035$$

$$\omega_n = 2\pi \times (155\ \text{KHz})$$

$$\omega_o = 2\pi \times (154.9\ \text{KHz})$$

$$\omega_{max} = 2\pi \times (154.8\ \text{KHz})$$

$$Q = 14.2$$

$$v_2(t) = .234 \times 10^{12} \exp(-2\pi \times 5.42 \times 10^3 t) \sin(2\pi \times 154.9 \times 10^3 t)u(t) \qquad (61)$$

$$v_1(t) = 948\,\delta(t) - \Big\{6.52 \times 10^6 \exp(-2\pi \times 5.42 \times 10^3 t) \times \Big[\cos(2\pi \times 154.9 \times 10^3 t) - 0.035 \sin(2\pi \times 154.9 \times 10^3 t)\Big]\Big\}.u(t) \qquad (62)$$

Plots of (59), (60), (61) and (62) for t varying from 0 to 50 μsec are shown on Graphs VI and VII. Since the system is linear, the magnitudes of these plots are proportional to the magnitude of the input impulse. For purpose of convenience we assume arbitrarily for these plots an input current impulse equal to 1 μA.

From those plots we note that the time constant, i.e., the rate of decay of the envelop, is approximately equal to 28 μsec while the pseudo-period of the waveform is 6.5 μsec.

For an input current impulse equal to 1 μA, the energy E_1 dissipated across the resistor R and the energy E_2 appearing at the input of the preamplifier are given by

$$E_1 = \int_{-\infty}^{\infty} \frac{v_1^2(t)\ dt}{R} \tag{63}$$

$$E_2 = \int_{-\infty}^{\infty} \frac{v_2^2(t)\ dt}{R} \tag{64}$$

Inspection of (63) and (64) after substituting for $v_1(t)$ and $v_2(t)$ using (59), (60), (61) and (62), tells us that these integrals can be written in the form $\int_0^{\infty} \sum_{i=1}^{N} (A_i e^{-\sigma_i t} \cos \omega_i t + B_i e^{-\sigma_i t} \sin \omega_i t).dt = \sum_{i=1}^{N} \left(\frac{A_i \sigma_i + B_i \omega_i}{\sigma_i^2 + \omega_i^2}\right)$ which is clearly convergent. Using numerical values, we found:

a) For $G_o = 0$

$$E_1 = 32.5\ \mu J \tag{65}$$

$$E_2 = 418\ \mu J \tag{66}$$

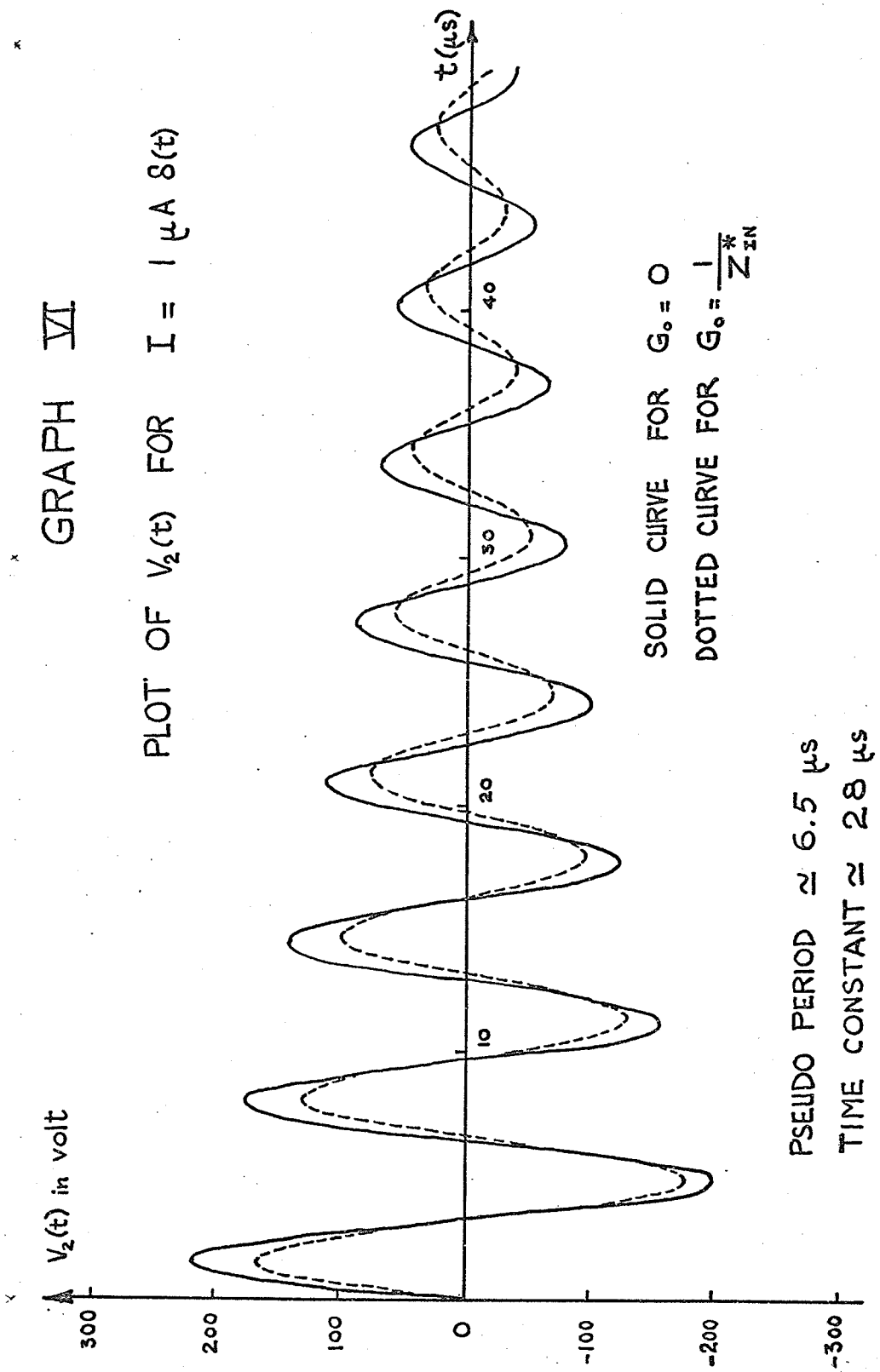
GRAPH VI
PLOT OF $V_2(t)$ FOR I = 1 μA δ(t)
$V_2(t)$ in volt
300
200
100
0
-100
-200
-300
10
20
30
40
t(μs)
SOLID CURVE FOR $G_0 = 0$
DOTTED CURVE FOR $G_0 = \frac{1}{Z^*_{IN}}$
PSEUDO PERIOD ≃ 6.5 μs
TIME CONSTANT ≃ 28 μs

GRAPH VII

PLOT OF $V_1(t)$ FOR $I = 1\ \mu A\ \delta(t)$

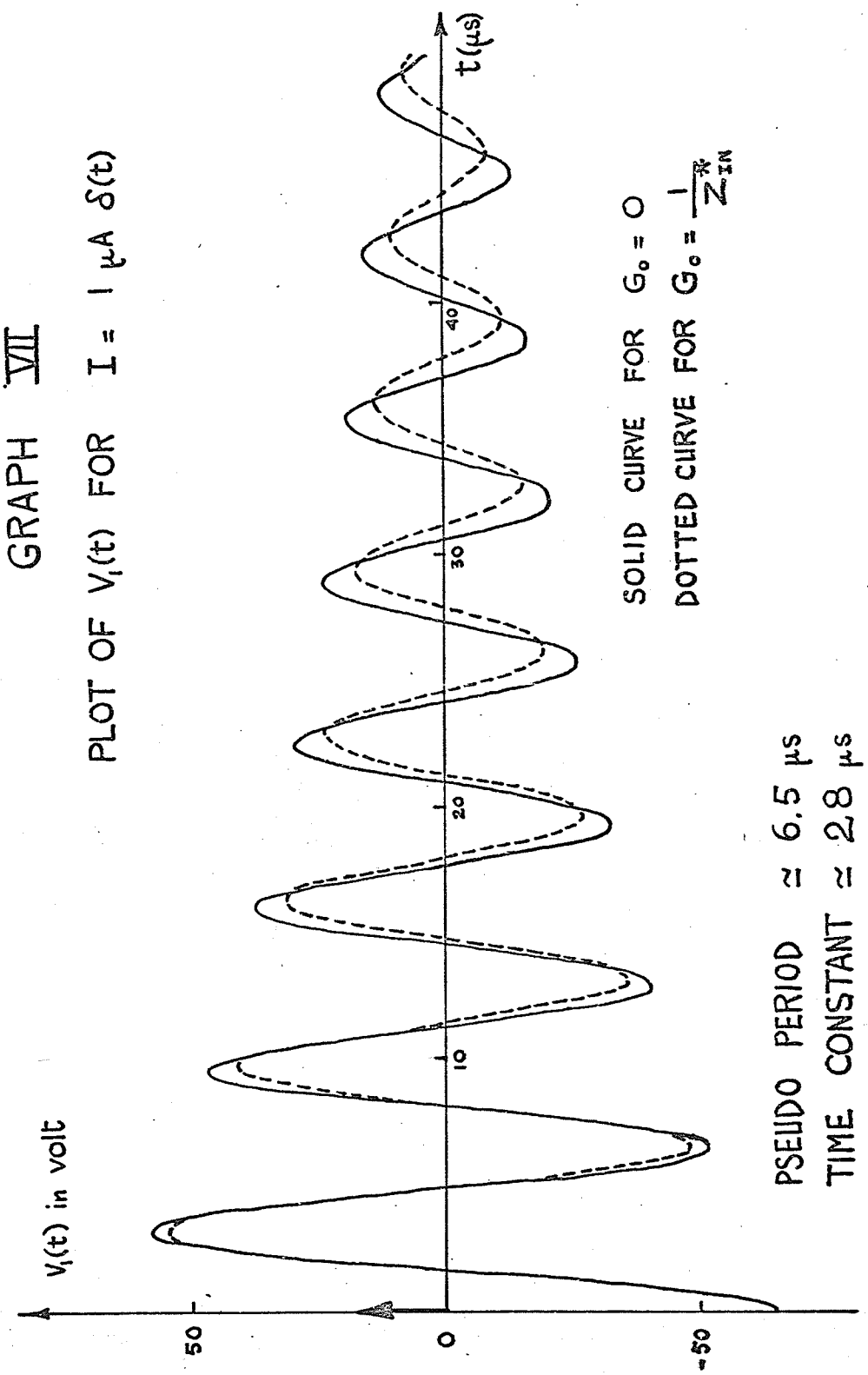

SOLID CURVE FOR $G_0 = 0$

DOTTED CURVE FOR $G_0 = \frac{1}{Z_{IN}}$

PSEUDO PERIOD $\simeq 6.5\ \mu s$

TIME CONSTANT $\simeq 28\ \mu s$

NOTE : THE IMPULSE AT $t = 0$ IS DRAWN OUT OF SCALE

b) For $G_o = 1/Z^*_{IN}$

$$E_1 = 25.3\ \mu J \tag{67}$$

$$E_2 = 248\ \mu J \tag{68}$$

We note that these quantities are proportional to the square of the intensity of the input current impulse.

B. Impulse Response of The System

In order to calculate the impulse response of the system, we need to know the transfer function G(s) of the preamplifier. A method for the gain and phase measurement of the preamplifier is shown in Fig. 18. The gain $\left|\frac{V_o(\omega)}{V_2(\omega)}\right|$ is plotted on Graph VIII and the phase difference $\angle\theta_2 - \angle\theta_o$ is plotted on Graph IX.

A model for the transfer function is required. Using Bode's design principles [10], we suggest the following expression:

$$G(s) = \frac{V_o(s)}{V_2(s)} = \frac{B\,s^3}{(s+s_6)(s+s_7)(s+s_8)(s^2+2\zeta_6 s_6 s+s_6^2)(s^2+2\zeta_7 s_7 s+s_7^2)(s^2+2\zeta_8 s_8 s+s_8^2)} \tag{69}$$

where

$$s_6 = 2\pi \times (105\ KHz) \quad ; \quad \zeta_6 = 0.35;$$

$$s_7 = 2\pi \times (320\ KHz) \quad ; \quad \zeta_7 = 0.35;$$

$$s_8 = 2\pi \times (750\ KHz) \quad ; \quad \zeta_8 = 0.60; \quad B = 2000 \times 0.7 \times 10^{39}$$

These values are derived from Graphs VIII and IX using a cut-and-try technique.

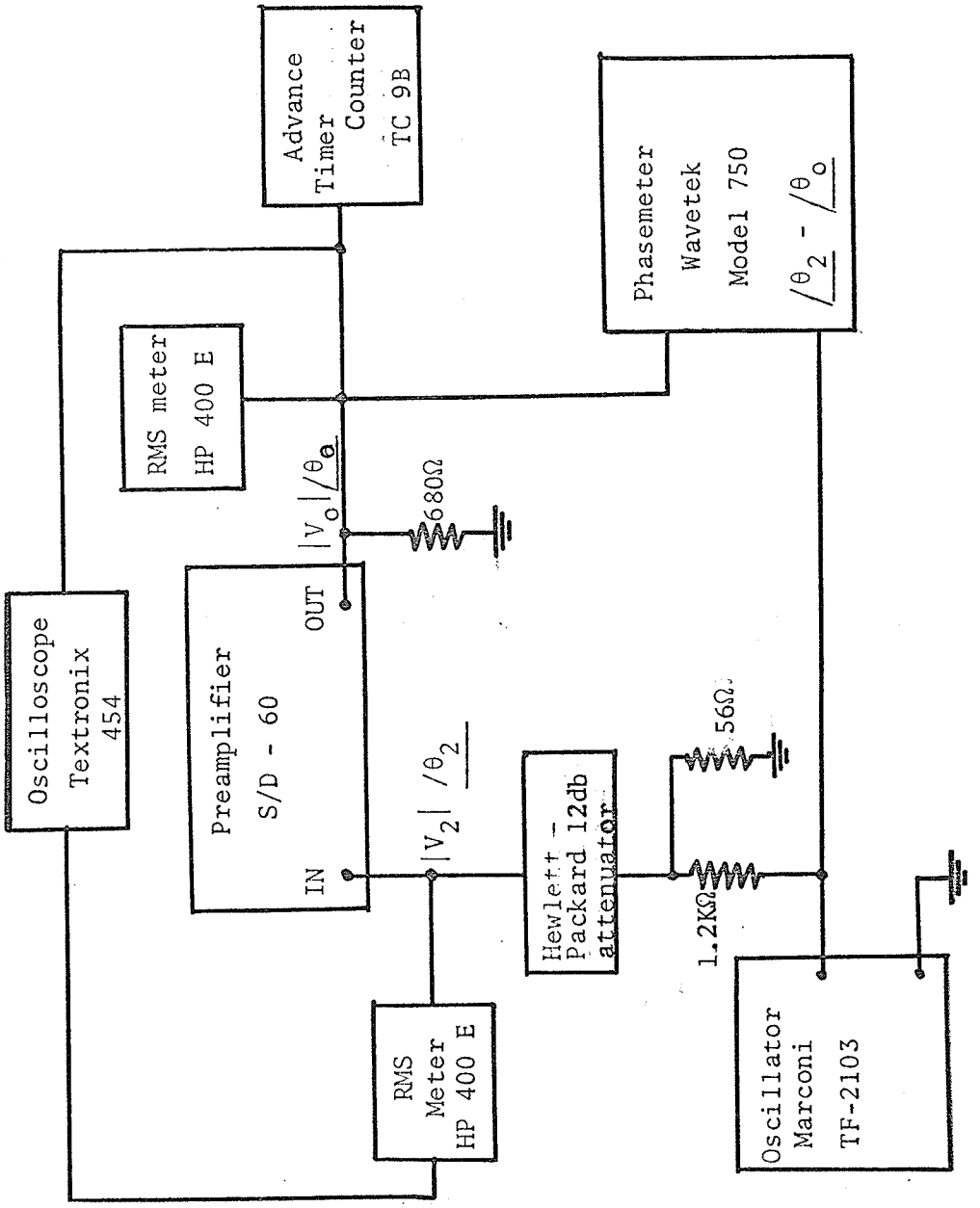

Fig. 18: Set-up for gain and phase measurement.

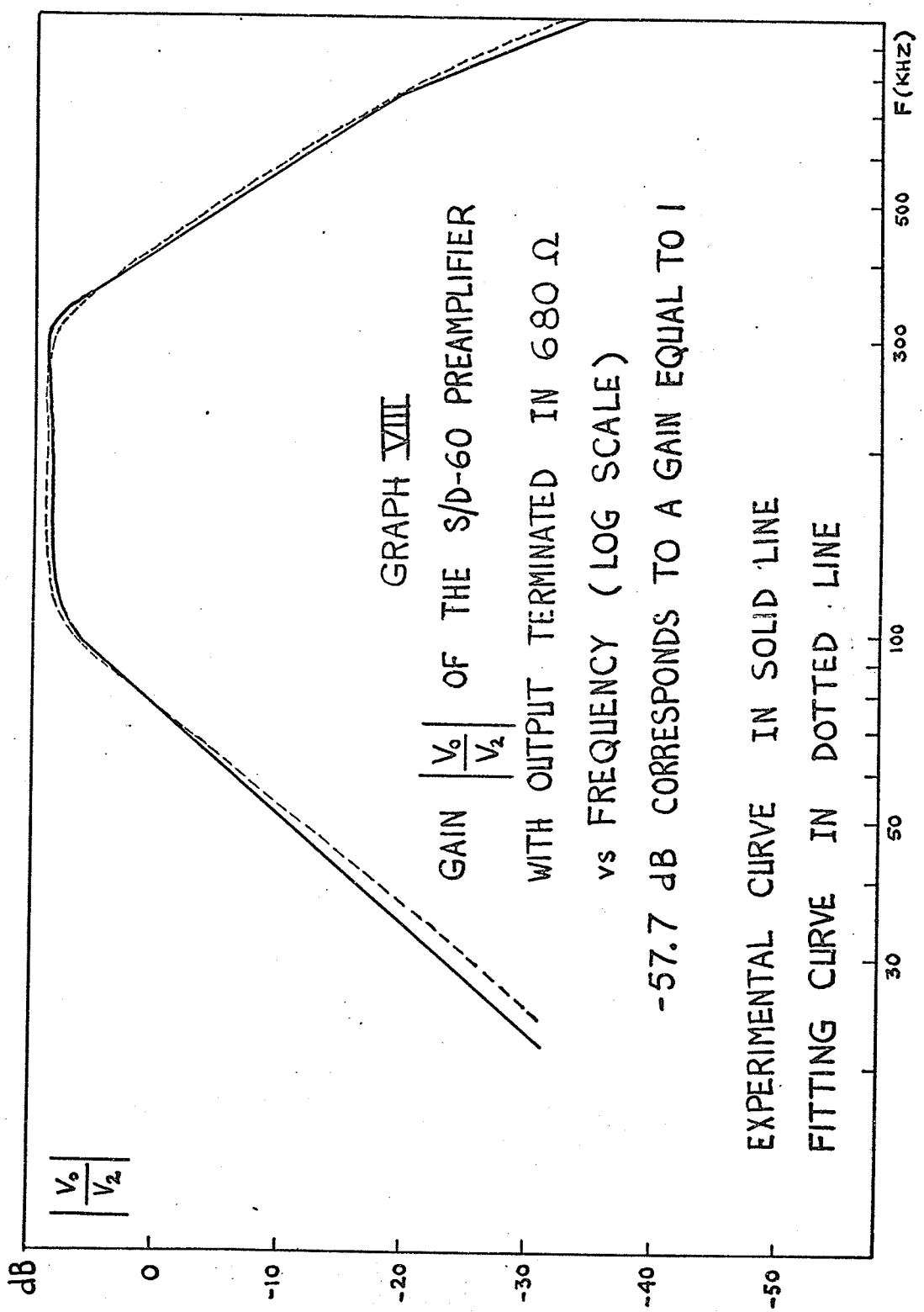
dB
0
-10
-20
-30
-40
-50
$\left|\frac{V_o}{V_2}\right|$
30
50
100
300
500
F(KHZ)
GRAPH VIII
GAIN $\left|\frac{V_o}{V_2}\right|$ OF THE S/D-60 PREAMPLIFIER
WITH OUTPUT TERMINATED IN 680 Ω
vs FREQUENCY (LOG SCALE)
-57.7 dB CORRESPONDS TO A GAIN EQUAL TO 1
EXPERIMENTAL CURVE IN SOLID LINE
FITTING CURVE IN DOTTED LINE

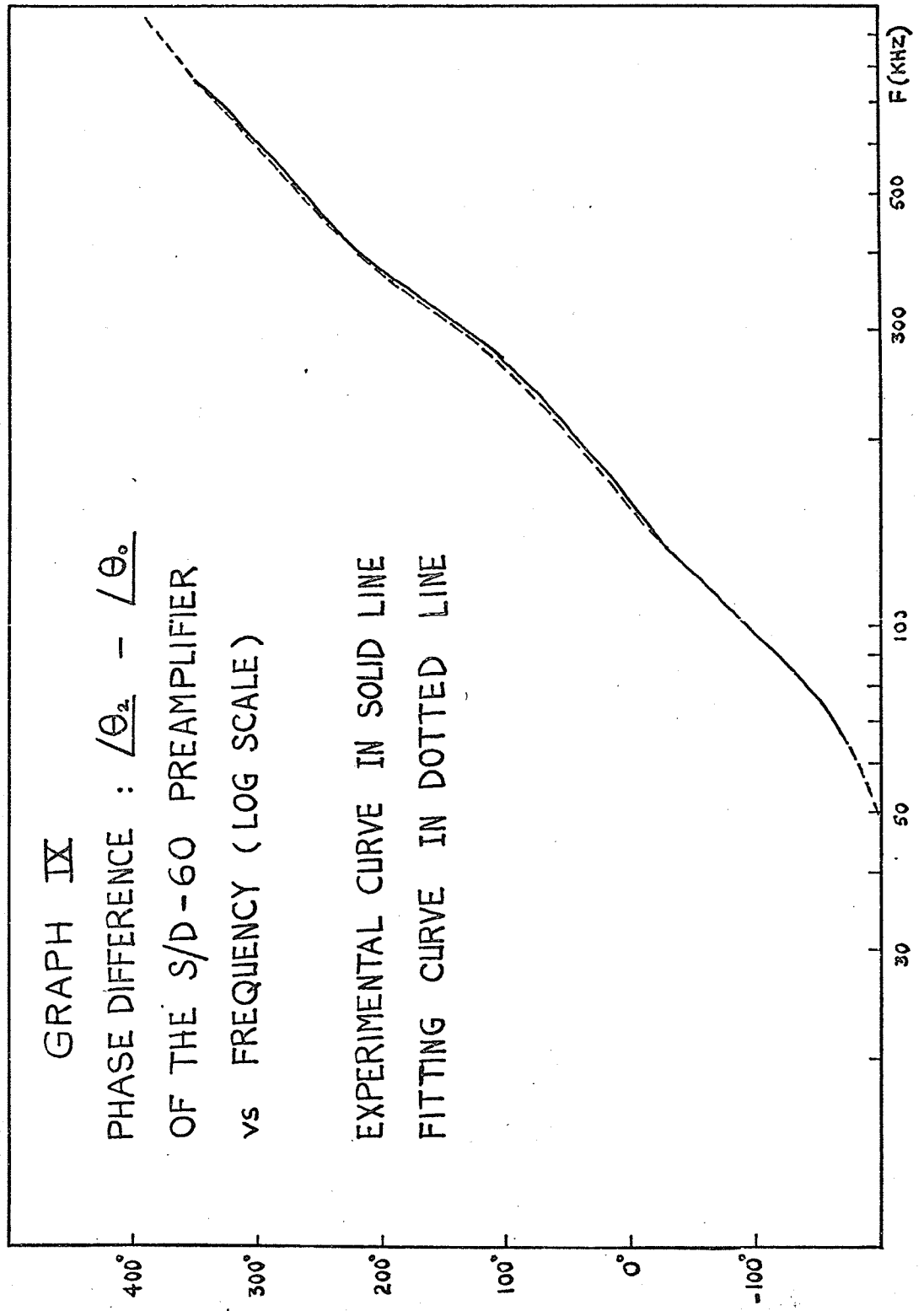
GRAPH IX
PHASE DIFFERENCE : ∠θ₂ - ∠θ₀
OF THE S/D-60 PREAMPLIFIER
vs FREQUENCY (LOG SCALE)
EXPERIMENTAL CURVE IN SOLID LINE
FITTING CURVE IN DOTTED LINE
400°
300°
200°
100°
0°
-100°
30
50
100
300
500
F(KHZ)

The accuracy of the phasemeter is 2°. The plot of the phase of (69) shows a maximum deviation of 6°. However, the model is judged satisfactory since the plot of the gain of (69) is within 0.5 db in the passband region. Therefore the overall transfer function is given by:

$$T(s) = \frac{V_o(s)}{I(s)} = \frac{V_2(s)}{I(s)} \cdot \frac{V_o(s)}{V_2(s)} = Z_{21}(s) \cdot G(s) \qquad (70)$$

where:

$Z_{21}(s)$ and $G(s)$ are given by (53) and (69).

Expressing (70) in dB, we have

$$20 \log |T(j\omega)| = 20 \log |Z_{21}(\omega)| + 20 \log |G(\omega)| \qquad (71)$$

Graph X shows the frequency response of the system with the amplifier excluded.

Setting $I(s) = 1$, we can write

$$V_o(s) = Z_{21}(s)\ G(s) = \sum_{i=1}^{14} \frac{L_i}{s - s_i} \qquad (72)$$

where all the s_i are already given and L_i are the residues of $V_o(s)$ at these poles.

In the time domain, we have

$$v_o(t) = \sum_{i=1}^{14} L_i\ e^{+s_i t} \qquad (73)$$

Solving for L_i and grouping complex conjugate terms, we get

$$v_o(t) = 0.268 \times 10^6 \exp(-0.2\ wt) - 0.217 \times 10^9 \exp(-1.05\ wt)$$

$$+ 0.367 \times 10^9 \exp(-3.2\ wt) - 0.112 \times 10^8 \exp(-7.5\ wt)$$

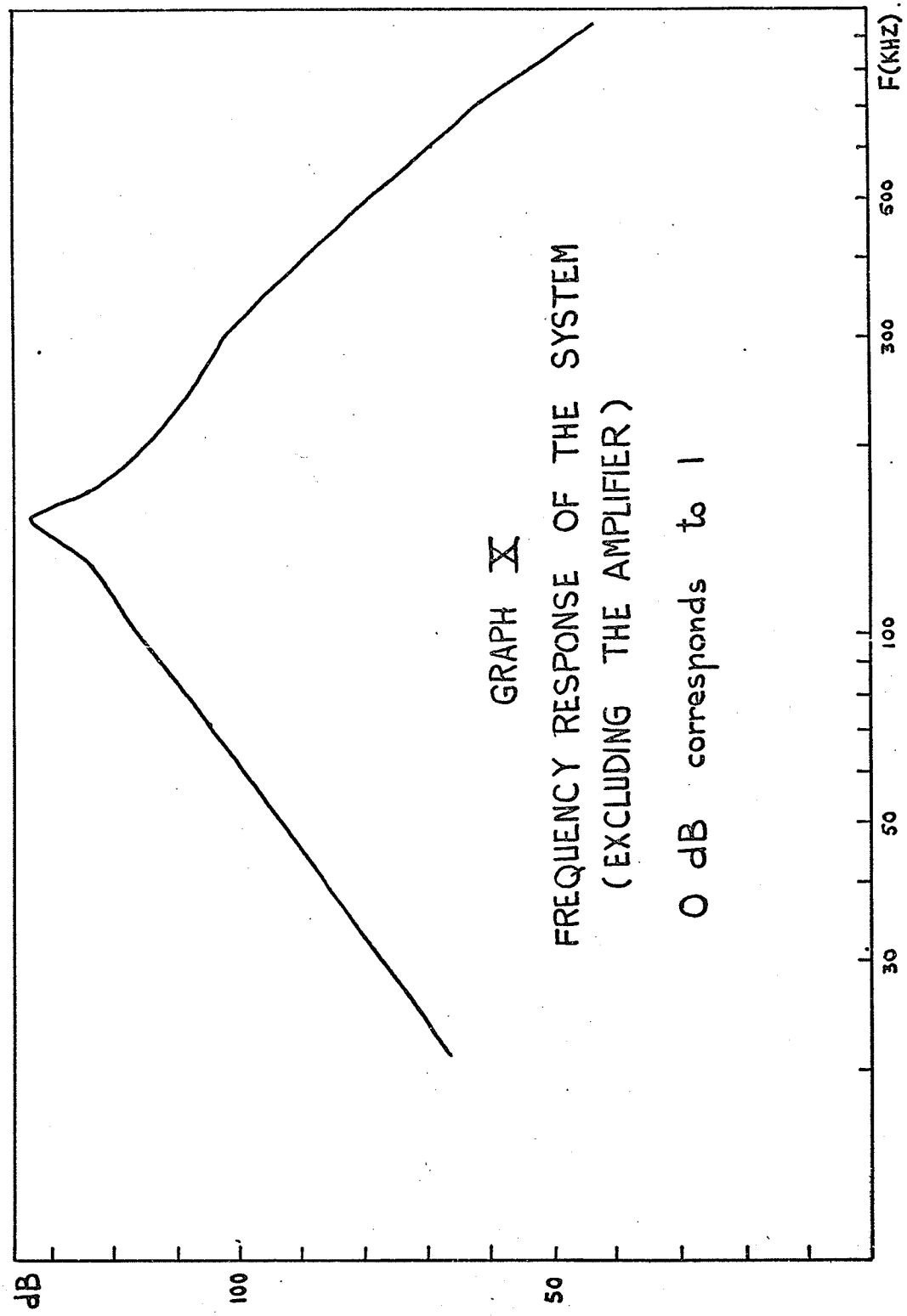

GRAPH X

FREQUENCY RESPONSE OF THE SYSTEM
(EXCLUDING THE AMPLIFIER)

0 dB corresponds to 1

$$+ 2\exp(-0.068\ wt)\left[0.103 \times 10^{8}\cos(1.52\ wt) + 0.118 \times 10^{9}\sin(1.52\ wt)\right]$$

$$+ 2\exp(-1.94\ wt)\left[-0.938 \times 10^{7}\cos(2.43\ wt) + 0.945 \times 10^{8}\sin(2.43\ wt)\right]$$

$$+ 2\exp(-0.367\ wt)\left[-0.124 \times 10^{9}\cos(0.98\ wt) - 0.254 \times 10^{8}\sin(0.98\ wt)\right]$$

$$+ 2\exp(-1.12\ wt)\left[0.504 \times 10^{8}\cos(3.0\ wt) + 0.160 \times 10^{8}\sin(3.0\ wt)\right]$$

$$+ 2\exp(-4.5\ wt)\left[0.412 \times 10^{7}\cos(6.0\ wt) + 0.149 \times 10^{7}\sin(6.0\ wt)\right]$$

where

$$w = 2\pi \times 10^{5} \tag{74}$$

Setting the input current impulse equal to 1 μA, we plot the impulse response for t varying from 0 to 50 μsec on Graph XI. From the plot, we see that the pseudo-period is about 7 μsec and the time constant approximately 25 μsec.

Since the amplifier has a wide bandwidth, we assume that the waveform of the impulse response of the system shown in Fig. 15 will have the same shape as $v_o(t)$ but a higher magnitude due to the gain K of the amplifier. Therefore, the pseudo-period and the time constant of the impulse response of the system will still be the same. A number of possible applications will be derived next from the knowledge of the impulse response $v_o(t)$.

C. Applications

1. Sensitivity of the transducer

From the photographs of the actual test on the Fe 3% Si specimen,

GRAPH XI

IMPULSE RESPONSE OF THE SYSTEM $V_o(t)$

FOR $I = 1\ \mu A\ \delta(t)$

$V_o(t) = 2000\ V(t)$

2000 is the nominal gain of the preamplifier

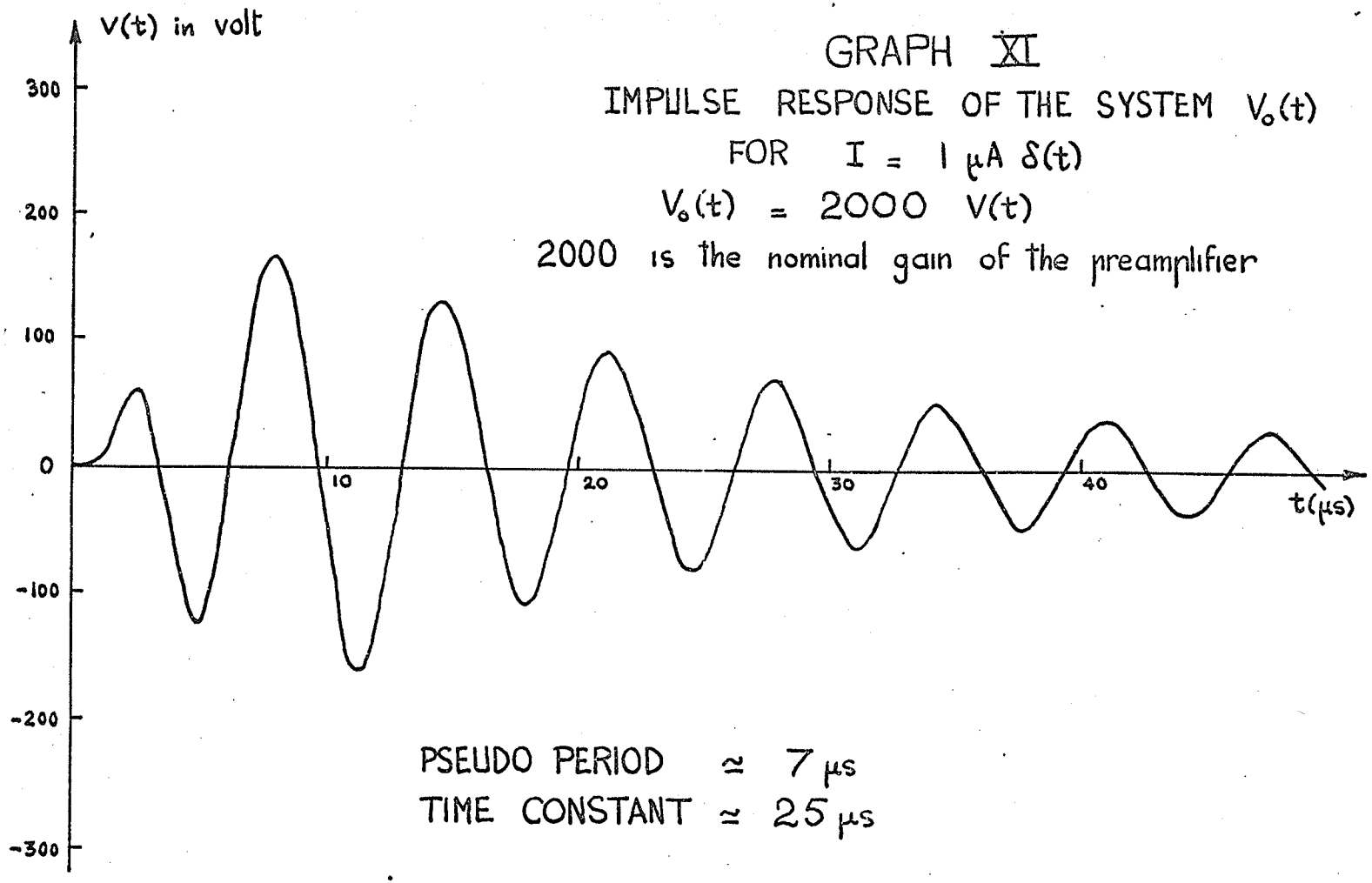

PSEUDO PERIOD $\simeq 7\ \mu s$

TIME CONSTANT $\simeq 25\ \mu s$

we notice that an acoustic emission is observable if its level is higher than the background noise of the preamplifier estimated to be equal to 5 μv at the input of the preamplifier therefore an acceptable level for an acoustic emission would be 10μv per example. From the plot of $v_o(t)$, such a level is generated by a current impulse of intensity

$$\frac{10v^{-5} \times 10^{-6} \text{ A}}{160 \text{ v}} \simeq \cdot 6 \times 10^{-13} \text{ A}$$

If by some method we are able to calibrate the transducer, i.e., to find the transformation factor relating the mechanical force to the electrical current, this quantity would give us the minimum strength of the force impulse which produces an observable acoustic emission.

2. Input and Output Waveforms

From what has been shown, we can simplify the overall system shown in Fig. 15 by the following (Fig. 19)

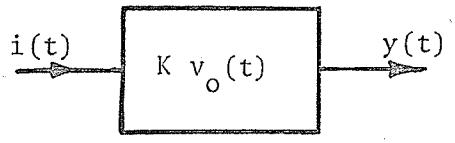

Fig. 19. Simplified model of the system.

where

i(t) is the input current which is the electrical equivalent of the input force.

$Kv_o(t) = v_{oo}(t)$ is the overall impulse-response and

$y(t)$ is the output waveform stored on tape.

From a linear system point of view [11], knowledge of $y(t)$ and $v_{oo}(t)$ leads to knowledge of $i(t)$ since

$$y(t) = \int_{-\infty}^{\infty} i(t_1)\, v_{oo}(t - t_1)\, dt_1 \tag{75}$$

This convolution integral in the time domain corresponds to a multiplication in the frequency domain:

$$Y(s) = I(s)\, V_{oo}(s) \tag{76}$$

where

$Y(s)$ is the Laplace transform of $y(t)$,

$I(s)$ is the Laplace transform of $i(t)$, and

$V_{oo}(s)$ is the Laplace transform of $v_{oo}(t)$

From (76), we obtain

$$I(s) = \frac{Y(s)}{V_{oo}(s)} \tag{77}$$

The inverse transform of (77) will give $i(t)$ in the time domain which is the input waveform corresponding to the observable output waveform.

Observed output waveforms resulting from the acoustic emission from Fe 3% Si specimens under tensile stress are shown by the photographs A, B, C and D on pp. 54-55.

From these photographs we may deduce that

a) The input waveform is a sequence of short pulses (i.e. transient waveform approaching an impulse) of random amplitude occurring at random time.

b) A main event may be accompanied by secondary events. We may

visualize this fact by considering an acoustic emission from a random source shown in Fig. 20, the secondary events result from multiple reflection and refraction as shown in Fig. 20. A possible corresponding input waveform could be the one shown in Fig. 21. Note that a main event may be by itself a superposition of simultaneous main events which come from other random sources for example.

c) However, if it happens that the secondary events are of minor importance, i.e., the first pulse corresponding to the main event is much greater than the accompanying pulses, in that case

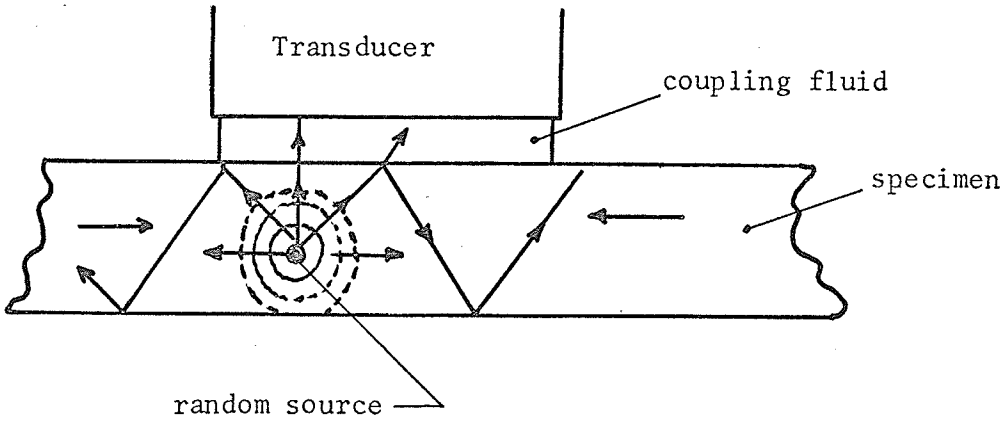

Fig. 20. Multiple reflection and refraction of an acoustic emission.

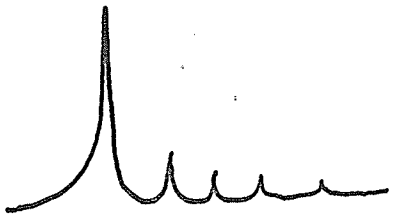

Fig. 21. A possible input waveform corresponding to the acoustic emission in Fig. 20.

Photograph A: Actual output waveform

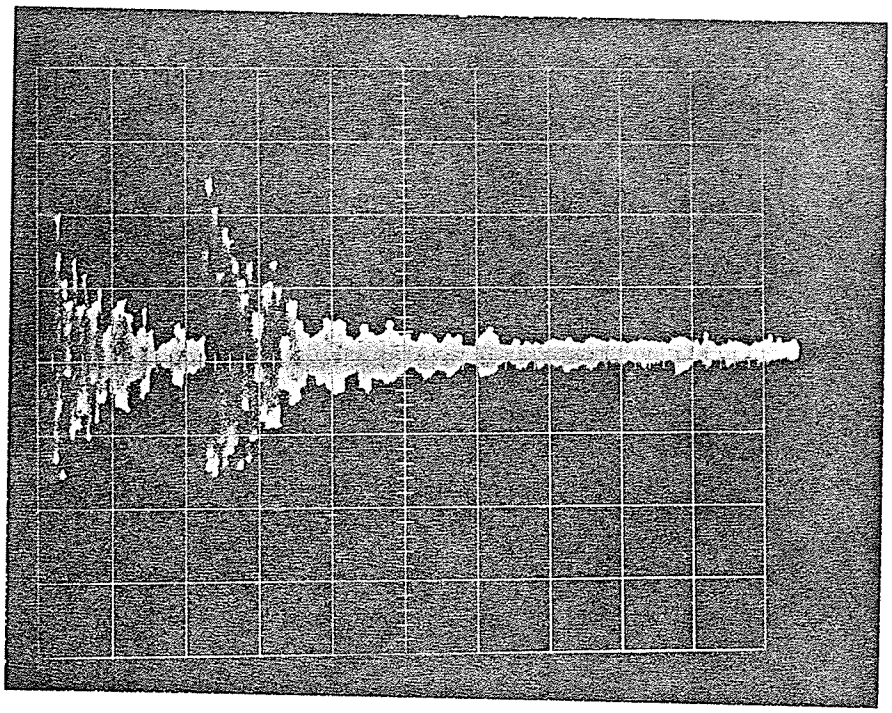

60 μv/cm

50 μsec/cm

Observed output waveforms resulting from the acoustic emission from Fe 3% Si specimens under tensile stress.

Photograph B: Actual output waveform

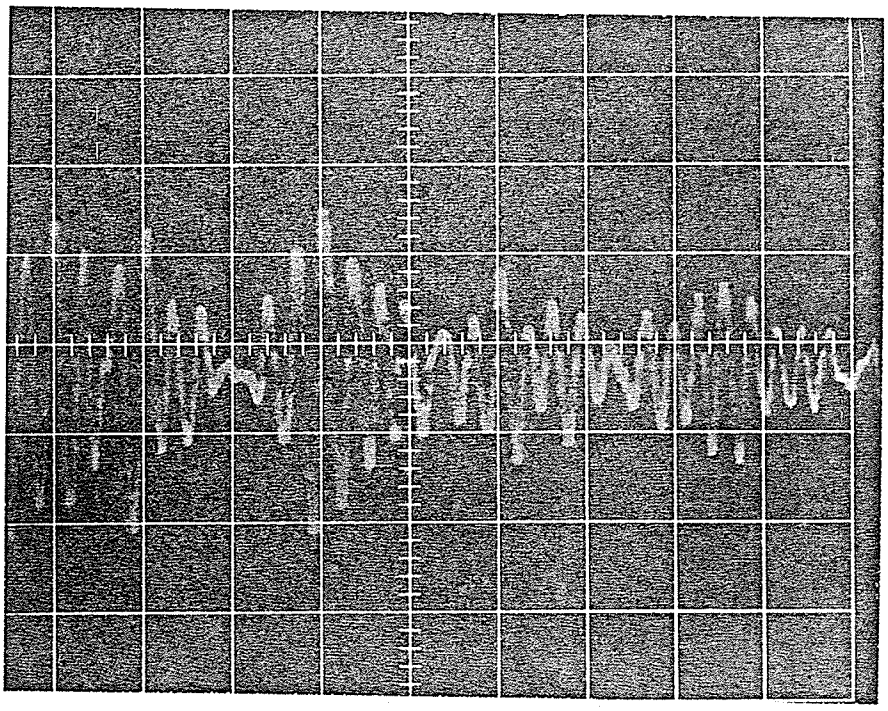

60 μv/cm

20 μsec/cm

Photograph C: Actual Output Waveform

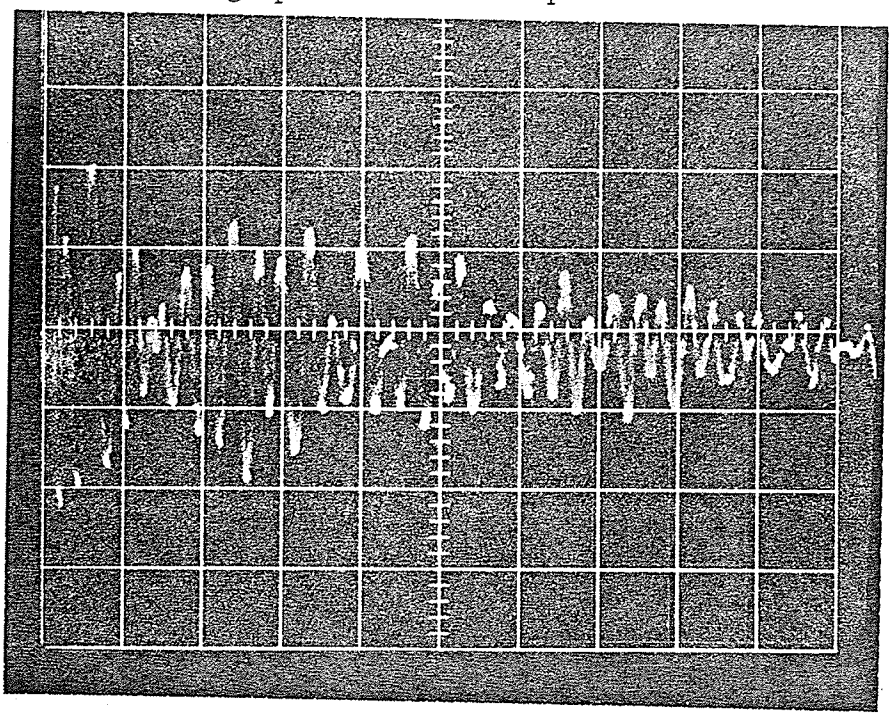

60 μv/cm

20 μsec/cm

Observed output waveforms resulting from the acoustic emission from Fe 3% Si specimens under tensile stress.

Photograph D: Actual output waveform

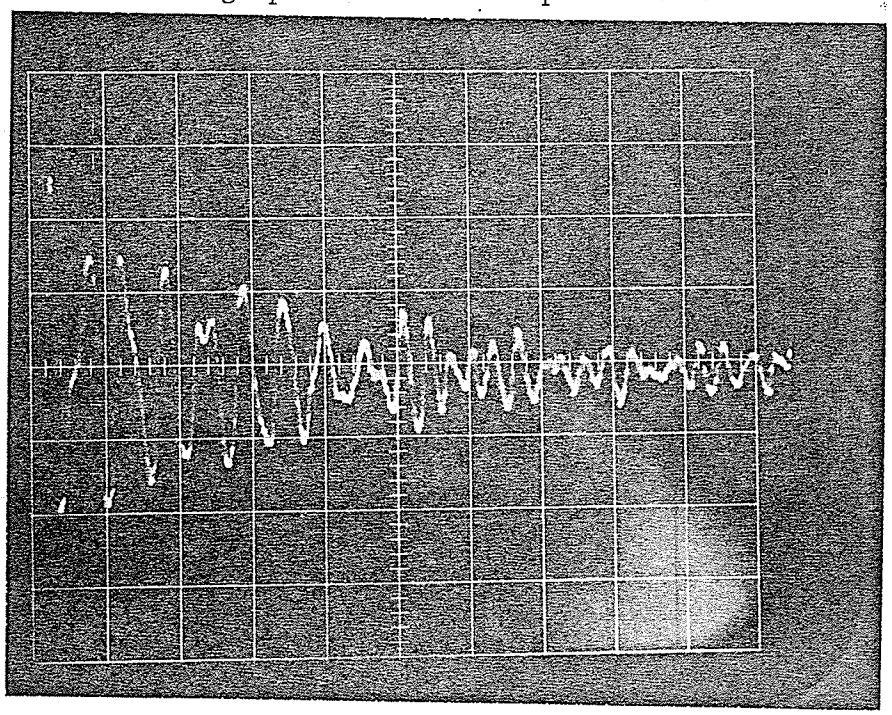

60 μv/cm

20 μsec/cm

we may count it as a single event. This assumption will permit us to check our electrical model. From photograph (A) we notice that the rate of decay of the two damped waveforms is approximately equal to 25 μsec. The same value is obtained from the second damped waveform starting at one division to the left of the vertical center line of photograph (B). Photograph (B), (C) and (D) show us a pseudo-period which is approximately equal to 7 μsec though some portions of these have a greater period which is due to a possible superposition of overlapping waveforms.

These values do check with the theoretical values we have found earlier. Therefore, they confirm our model favorably.

3. Input and Output Statistical Properties

From the previous deductions, we expect that the acoustic emission is a stochastic process. The study of such a process requires the determination of the statistical properties of the input as well as of the output. Knowledge of $v_{oo}(t)$ will generally enable us to find the statistical properties of the output from the statistical properties of the input. (As an illustrative example, one can refer to the shot noise problem which has been solved by Rice [12], Laning and Battin [13]). We consider the converse since the statistical properties of the input are unknown. In the frequency domain we have the following relation [14]:

$$G_{yy}(\omega) = |V_{oo}(\omega)|^2 \, G_{xx}(\omega) \tag{78}$$

where $G_{yy}(\omega)$ and $G_{xx}(\omega)$ are respectively the spectral density of the output and of the input waveform. Hence, it is possible to find $G_{xx}(\omega)$ from $G_{yy}(\omega)$ and $v_{oo}(t)$. Then one may derive the autocorrelation function by taking the inverse Fourier transform of the spectral density; the mean value and the mean square value can be found from the correlation function.

But the probability density of the input is in general difficult to find from the probability density of the output.

If the input waveform is a sequence of short pulses, then we may use an envelop detector to count the rate of occurrence of these pulses. This technique has the following drawbacks:

- If the interval between two pulses in too small, i.e. much smaller than the time constant of $v_o(t)$, the resulting output waveforms will overlap and the count may be taken as one single pulse.
- The diodes used in the envelop detector are not ideal and as a result low level signals are eliminated.

Obviously, the input waveform may be more complicated and one may expect that in general the process is not stationary which makes the determination of the statistical properties more difficult. In fact, Bendat and Piersol [15] point out that a totally adequate methodology does not exist as yet for the analysis of all types of nonstationary data. Since the statistical properties of the process are time-dependent, this situation would require on-line computation technique for the probability density function, the autocorrelation function and the power spectral density function.

CHAPTER IV

CONCLUSIONS

A method of modeling a transducer used in the study of acoustic emission from materials under tensile stress has been presented in this thesis. First, we measure the impedance of the transducer over a wide range of frequencies and then use this experimental data to solve two nonlinear equations which determine the model parameters. As an illustrative example, we have applied the technique to determine the electrical model for an actual transducer. The result is quite satisfactory since the fitting impedance curve closely approximates the experimental impedance curve (Graphs I and II).

The validity of the technique is subject to a constraint, i.e., the transducer must not have other modes of resonance near its main resonance. This constraint is not important in practice since transducers are designed such that their principal mode of resonance is well isolated from the other possible modes in the frequency band of interest. Thus in our present study, we have neglected, for example, minor resonances which occur outside the band of frequencies 100 KHz to 300 KHz. On the other hand, the accuracy of the acceptable model could be improved by more accurate measuring equipment. Modeling the input impedance and the preamplifier permits us to calculate the impulse response of the system which in turn allows us to calculate the input waveform from the observed output waveform. For example, the input waveshape and the input statistical properties may be obtained from the output waveform and from the output statistical properties once the impulse response has been found. In particular, the pseudo period and the time constant of the calculated

impulse response agree favorably with the actual output waveform. Thus, the present modeling method proposed can be applied adequately to signal analysis of the system.

However, some problems remain to be considered: such as the investigation of the statistical properties of the output waveform, the investigation and the interpretation of the input waveform in terms of the physical behavior of the material in the specimen and the investigation of a possible relation between certain statistical properties of the output and the strain rate. Further, we would suggest the investigation of the possibility of generating an acoustic random white noise or pseudo random binary sequence in order to determine by a cross-correlation method [16] the impulse response of the system without requiring a circuit model for the preamplifier. Finally, the development of a method to determine the transformation factor between force and current intensity for the transducer should be considered; since the current source is the analog of the mechanical force, such a determination would let us to interpret the results either in mechanical units or in electrical units.

REFERENCES

1. W.P. Mason, Electromechanical transducers and wave filters, 2d Ed. New York: D. Van Nostrand, 1948, pp. 195-209.
2. W.P. Mason, Physical Acoustics, Vol. I, Part A. New York: Academic Press, 1964, pp. 170-246.
3. L.L. Beranek, Acoustics. New York: McGraw-Hill, 1954, pp. 47-90.
4. L.E. Kinsler and A.R. Frey, Fundamentals of Acoustics, 2d Ed. New York: Wiley, 1967, pp. 333-364.
5. W.G. Cady, Piezoelectricity, 2d Ed. New York: Dover, 1964.
6. "IRE Standards on Piezoelectric Crystals", Proc. IRE Vol. 45, March 1957, pp. 354-358.
7. E. Hafner, "The piezoelectric crystal unit: Definitions and Methods of Measurement", Proc. IEEE Vol. 57, Feb. 1969, pp. 179-200.
8. W.D. George and M.C. Selby, "Precision Measurement of Electrical Characteristics of quartz crystal units", Proc. IRE Vol. 36, September 1948, pp. 1122-1131.
9. F.K. Kuo, Network Analysis and Synthesis, 2d Ed, New York: Wiley, 1966, pp. 229-233.
10. K. Ogata, Modern Control Engineering, New Jersey: Prentice-Hall, 1970, pp. 451-455.
11. G.R. Cooper and C.D. McGillem, Methods of Signal and System Analysis. New York: Holt, Rinehart and Winston, 1967, pp. 196-199.
12. S.O. Rice, "Mathematical Analysis of Random Noise", Bell System Tech. J. Vol. 23, pp. 283-332, July 1944; Vol. 24, pp. 46-156, January 1945.
13. J.H. Laning and R.H. Battin, Random Processes in Automatic Control.

14. Y.W. Lee, Statistical Theory of Communication Theory. New York: Wiley, 1960, pp. 323-351.

15. J.S. Bendat and A.G. Piersol, Measurement and Analysis of random data. New York: Wiley, 1968, pp. 333-377.

16. R.L. Rex and G.T. Roberts, "Correlation, Signal averaging, and Probability Analysis", Hewlett-Packard Journal Vol. 21, November 1969, pp. 2-8.

17. J.S. Bendat, Principles and Applications of Random noise Theory. New York: Wiley, 1958.

18. J. Blitz, Fundamentals of Ultrasonics. London: Butterworths, 1963, pp. 40-60.

19. F.E. Terman, Radio Engineering 3rd Ed. New York: McGraw-Hill, 1947, pp. 418-426.